A Simple Mesh Free Model for Static Analysis of Smart Composite Beams

Divyesh mistry

A Simple Mesh Free Model for Static Analysis of Smart Composite Beams

Thesis submitted to
Indian Institute of Technology Kharagpur
For the award of the degree

Of

Master of Technology in Mechanical Systems Design

By

Divyesh Mistry
Roll No. 14ME63R02

Under the guidance

of

Prof. Manas Chandra Ray

DEPARTMENT OF MECHANICAL ENGINEERING
INDIAN INST ITUTE OF TECHNOLOGY KHARAGPUR
DECEMBER, 2015

Department of Mechanical Engineering

Indian Institute of Technology Kharagpur

APPROVAL OF THE VIVA-VOCE BOARD

December 2015

Certified that the thesis entitled "A Simple Mesh Free Model for Static Analysis of Smart Composite Beams" submitted by Divyesh Arjunbhai Mistry (14ME63R02) to the Indian Institute of Technology, Kharagpur, for the award of the degree Master of Technology in Mechanical Systems Design has been accepted by the external examiner and that the student has successfully defended the thesis in the viva-voce examination held today.

_____

Prof. Manas Chandra Ray

Department of Mechanical Engineering Indian

Institute of Technology, Kharagpur

_____

(External Examiner)

_____

(Course Coordinator)

I certify that

a. The work contained in the thesis is original and has been done by myself under the general supervision of my supervisor.

b. The work has not been submitted to any other Institute for any degree or diploma.

c. I have followed the guidelines provided by the Institute in writing the thesis.

d. I have conformed to the norms and guidelines given in the Ethical Code of Conduct of the Institute.

e. Whenever I have used materials (data, theoretical analysis, and text) from other sources, I have given due credit to them by citing them in the text of the thesis and giving their details in the references.

f. Whenever I have quoted written materials from other sources, I have put them under quotation marks and given due credit to the sources by citing them and giving required details in the references.

Divyesh Mistry
(14ME63R02)

ABSTRACT

Piezoelectric laminated beams are common piezoelectric structure. It has been applied in many fields, such as the driving element of the bimorph and unimorph piezoelectric actuators bending. For static and dynamic, linear and nonlinear, analytical method and numerical method, the mechanical behaviors of this structure (including bending, vibration, buckling and control, etc.) have very comprehensive research. In these studies, most of the research is to use of laminated beam theory simplified into 1D control equation. However, here we will adopt a new approximate method based on Element free Galerkin (EFG) for the numerical simulation of piezoelectric laminated beam. This new meshfree method can overcome the material discontinuity between layer and thickness lock phenomenon. This new method is suitable for thin beam and thick beam. It can be generalized to the numerical calculation of laminated curved beam, laminated plate and shell structures. Numerical examples verify the validity and precision of the proposed method.

KEY WORDS : Piezoelectric; Meshfree method; Element Free Galerkin; Laminated beam

NOMENCLATURE

[C]	Elastic constant matrix
$[\boldsymbol{e}]$	Piezoelectric constant matrix
{D}	Electric displacement vector
{E}	Electric field vector
$\{\boldsymbol{\varepsilon}\}$	Strain vector
$\{\boldsymbol{\sigma}\}$	Stress vector
$\boldsymbol{u}, \boldsymbol{v}, \boldsymbol{w}$	Displacement components along x, y and z axes
{d}	Generalized displacement variable
$\boldsymbol{\sigma_x}, \boldsymbol{\sigma_y}, \boldsymbol{\sigma_z}, \boldsymbol{\sigma_{xy}}, \boldsymbol{\sigma_{xz}}, \boldsymbol{\sigma_{yz}}$	Stress components
$\boldsymbol{\varepsilon_x}, \boldsymbol{\varepsilon_x}, \boldsymbol{\varepsilon_x}, \boldsymbol{\gamma_{xy}}, \boldsymbol{\gamma_{xz}}, \boldsymbol{\gamma_{yz}}$	Strain components
$\boldsymbol{\sigma_x^p}, \boldsymbol{\sigma_y^p}, \boldsymbol{\sigma_z^p}, \boldsymbol{\sigma_{xy}^p}, \boldsymbol{\sigma_{xz}^p}, \boldsymbol{\sigma_{yz}^p}$	Stress components for piezo
$\boldsymbol{\varepsilon_x^p}, \boldsymbol{\varepsilon_y^p}, \boldsymbol{\varepsilon_z^p}, \boldsymbol{\gamma_{xy}^p}, \boldsymbol{\gamma_{xz}^p}, \boldsymbol{\gamma_{yz}^p}$	Strain components for piezo
u_0, v_0, w_0	Generalized translation displacement
θ_x, θ_y	Generalized rotational displacement
[N]	Shape function matrices
$[e]$	Matrices of piezoelectric constants
Π	Total potential energy of plate
{f}	Externally applied surface traction vector
[H]	Nodal generalized strain/ displacement Matrices
$[K]$	Global Stiffness matrices
$[F^e]$	The elemental load vector

$\mathbf{a}$,$\mathbf{b}$	Length and width of element.
d_s	Average nodal spacing
α_s	Dimensionless size of the support domain
A_s	Area of support domain
V_s	Volume of support domain
$u(x)$	Field variable
$P(x)$	Basis function
$a(x)$	Vector of coefficients
$\widehat{W}(x-x_i)$	Weight function
$\boldsymbol{\psi}(\boldsymbol{x})$	Shape function
$\boldsymbol{\lambda}$	Lagrange multiplier
$\boldsymbol{\sigma_x^k}$	Normal stress along the $\mathbf{x}$-direction
$\boldsymbol{\sigma_z^k}$	Normal stress along the $\mathbf{z}$-direction
$\boldsymbol{\sigma_{xz}^k}$	Transverse shear stress
$\boldsymbol{\phi_i}$	The nodal electric potential parameter
$\mathbf{[F_p]}$	Electro-elastic coupling matrix

LIST OF FIGURES

TABLE OF CONTENTS

TABLE OF CONTENTS

1. INTRODUCTION

The problems of computational mechanics grow ever more challenging for example in the simulation of manufacturing processes such as extrusion and molding it is necessary to deal with extremely large deformations of the mesh while in computations of castings the propagation of interfaces between solids and liquids is crucial. In simulations of failure processes we need to model the propagation of cracks with arbitrary and complex paths in the development of advanced materials methods which can track the growth of phase boundaries and extensive micro-cracking are required. The finite element method for the modeling of complex problems in applied mechanics and related fields is well established. It is a robust and thoroughly developed technique, but it is not without shortcomings. The reliance of the method on a mesh leads to complications for certain classes of problems. Consider the modeling of large deformation processes; considerable loss in accuracy arises when the elements in the mesh become extremely skewed or compressed. The growth of cracks with arbitrary and complex paths, and the simulation of phase transformations is also difficult. The use of a mesh in modeling these problems creates difficulties in the treatment of discontinuities which do not coincide with the original mesh lines. The traditional technique for handling these complications is to remesh the domain of the problem at every step during the evolution of the simulation. This prevents the severe distortion of elements and allows mesh lines to remain coincident with any discontinuities throughout the evolution of the problem. For this purpose, several complex and robust mesh generation routines have been developed. However, this technique requires the projection of field variables between meshes in successive stages of the problem, which leads to logistical problems as well as a degradation of accuracy. In addition, for large three dimensional problems, the computational cost of remeshing at each step of the problem becomes prohibitively expensive. To ameliorate these difficulties, a new class of methods have recently been

developed which do not require a mesh to discretize the problem. These are methods in which the approximate solution is constructed entirely in terms of a set of nodes, and no elements or characterization of the interrelationship of the nodes is needed to construct the discrete equations. It is then possible to develop discrete equations from a set of nodes and a description of the internal and external surfaces of the model. For the latter purpose, a CAD description, such as a model in three dimensions, may be used, so meshfree methods may overcome many of the difficulties associated with meshing for three-dimensional analyses.

1.1 Objective

- The main objective of this project is Static analyze of smart composite beam using Meshfree method.
- To define shape function construction for MFree method and Meshfree interpolation/approximation techniques.
- To derive the solution for smart composite beam.
- Comparison of Responses of Mfree Method for Three Layered (0/90/0) Composite Beam with Exact Solution Method.
- Comparison of Responses of Mfree Method for Four Layered (0/90/0/90) Composite Beam with Exact Solution Method.

1.2 Literature Review

The development of some of the MFree methods can be traced back more than seventy years to the collocation methods (Slater, 1934; Barta, 1937; Frazer et al., 1937; Lanczos, 1938, etc). Some of the early MFree methods were the vortex method (Chorin, 1973; Bernard, 1995), finite difference method (FDM) with arbitrary grids, or the general FDM (GFDM) (Girault, 1974; Pavlin and Perrone, 1975; Snell et al, 1981; Liszka and Orkisz, 1977; 1980; Krok and Orkisz, 1989). Another well-known MFree method is the Smoothed Particle Hydrodynamics (SPH) that was initially used for

modelling astrophysical phenomena such as exploding stars and dust clouds that had no boundaries. Most of the earlier research work on SPH is reflected in the publications of Lucy (1977), and Monaghan and his coworkers (Gingold and Monaghan, 1977; Monaghan and Lattanzio, 1985; Monaghan, 1992). Overall, there has been less research devoted to MFree strong-form methods. This may be partly because the MFree strong-form method was less robust than the method based on the weak-form, and partly because research was concentrated on the finite element method (FEM) which used weak-forms; it was then a natural step to MFree weak-form methods.

There has been substantial improvement in these methods. Swegle, Hicks, and Attaway (1995) have shown the origin of the so-called tensile instability through a dispersion analysis of the linearized equations and proposed a viscosity term to stabilize it. Dyka (1994) has proposed stabilization by means of stress particles Johnson and Beissel (1996) have proposed a method for improving the strain calculation Liu Jun and Zhang (1995) have proposed a correction function for kernels in both the discrete and continuous case. A parallel path to constructing meshless approximations which commenced much later is the use of moving least square approximations Nayroles (1992) were evidently the first to use moving least square approximations in a Galerkin method called the diffuse element method (DEM).

Belytschko Lu and Gu (1994) refined and modified the method and called their method EFG, element free Galerkin. These methods do not require a mesh at least for the field variable interpolations. The approximation functions are constructed by using a set of arbitrary nodes, and no element or connectivity of the nodes is needed for the function approximation. Adaptive analyses and simulations using MFree methods become very efficient and much easier to implement, even for problems which pose difficulties for the traditional FEM. In 1994, Belytschko et al. (1994) proposed the element free Galerkin (EFG) method in their important paper, in which the MLS approximation was used in the Galerkin weak-form to establish a set of algebraic equations. In the EFG method, the problem domain is represented by a set of properly

distributed nodes. The MLS approximation is used to construct shape functions based only on a group of arbitrarily distributed nodes in a local domain. A set of background cells are required to evaluate the integrals resulted from the use of the Galerkin weak-form. Belytschko and his colleagues have reported that the EFG method is very accurate (Belytschko, et al, 1994a; 1996a), and the rate of convergence of the EFG method obtained from numerical tests is higher than that of FEM (Belytschko, et al, 1994a). In addition, the irregularity of nodes does not affect the performance of the EFG method (Belytschko, et al, 1994a). The EFG method has been successfully applied to a large variety of problems including two-dimensional (2-D) and three-dimensional (3-D) linear and nonlinear elastic problems (Belytschko, et al, 1994a; Lu et al., 1994; Belytschko et al., 1997; Jun, 1996; Chen and Guo, 2001), fracture and crack growth problems (Belytschko, et al, 1994b; Belytschko, et al, 1995a, 1995b, 1995c; Krysl and Belytschko 1999; Lu et al., 1995), plate and shell structures (Krysl and Belytschko, 1995; 1996; GR Liu and Chen, 2000, 2001; Liu L and GR Liu et al., 2001, 2002a,b; Chen and GR Liu et al., 2001,2003).All these applications and extensions indicate that the EFG method is gradually becoming a mature and practical computational approach in the area of computational mechanics, thanks to the use of the MLS approximation to achieve stability in function approximation, and use of Galerkin procedure to provide stable and well behaved discretized global system equations.

2. MESHFREE METHOD

One of the most important advances in the field of numerical methods was the development of the finite element method (FEM) in the 1950s. In the FEM, a continuum with a complicated shape is divided into elements, finite elements. The individual elements are connected together by a topological map called a mesh. The FEM is a robust and thoroughly developed method, and hence it is widely used in engineering fields due to its versatility for complex geometry and flexibility for many types of linear and non-linear problems. Most practical engineering problems related to solids and structures are currently solved using well developed FEM packages that are commercially available. However, the FEM has the inherent shortcomings of numerical methods that rely on meshes or elements that are connected together by nodes in a properly predefined manner. The following limitations of FEM are becoming increasingly evident:

1) High cost in creating an FEM mesh

The creation of a mesh for a problem domain is a prerequisite in using any FEM code and package. Usually the analyst has to spend most of the time in such a mesh creation, and it becomes the major component of the cost of a computer aided design (CAD) project. Since operator costs now outweigh the cost of CPU (central processing unit) time of the computer, it is desirable that the meshing process can be fully performed by the computer without human intervention. This is not always possible without compromising the quality of the mesh for the FEM analysis, especially for problems of complex three-dimensional domains.

2) Low accuracy of stress

Many FEM packages do not accurately predict stress. The stresses obtained in FEM are often discontinuous at the interfaces of the elements due to the piecewise (or element-wise) continuous nature of the displacement field assumed in the FEM formulation.

3) Limitation in the analyses of some problems

- Under large deformations, considerable loss in accuracy in FEM results can arise from the element distortions.
- It is difficult to simulate crack growth with arbitrary and complex paths which do not coincide with the original element interfaces.
- It is very difficult to simulate the breakage of material with large number of fragments; the FEM is based on continuum mechanics, in which the elements cannot be broken; an element must either stay as a whole, or disappear completely. This usually leads to a misrepresentation of the breakage path

4) Difficulty in adaptive analysis

One of the current new demands on FEM analysis is to ensure the accuracy of the solution; we require a solution with a desired accuracy. To achieve this purpose, a so-called adaptive analysis must be performed. In an adaptive analysis using FEM, re-meshing (re-zoning) is required to ensure proper connectivity. For this re-meshing purpose, complex, robust and adaptive mesh generation processors have to be developed. These processors are limited to two-dimensional problems. Technical difficulties have precluded the automatic creation of hexahedron meshes for arbitrary three-dimensional domains. In addition, for three-dimensional problems, the computational cost of re-meshing at each step is very expensive, even if an adaptive scheme were available. Moreover, an adaptive analysis requires "mappings" of field variables between meshes in successive stages of the analysis. This mapping process can often lead to additional computation as well as a degradation of accuracy in the solution.

2.2 Definition of Meshfree Methods

The definition of an MFree method (GR Liu, 2002) is:

"An MFree method is a method used to establish system algebraic equations for the whole problem domain without the use of a predefined mesh for the domain discretization."

MFree methods use a set of nodes scattered within the problem domain as well as sets of nodes scattered on the boundaries of the domain to represent (not discretize) the problem domain and its boundaries. These sets of scattered nodes are called field nodes, and they do not form a mesh, meaning it does not require any a priori information on the relationship between the nodes for the interpolation or approximation of the unknown functions of field variables.

2.2.1 Solution Procedure of Mfree Methods

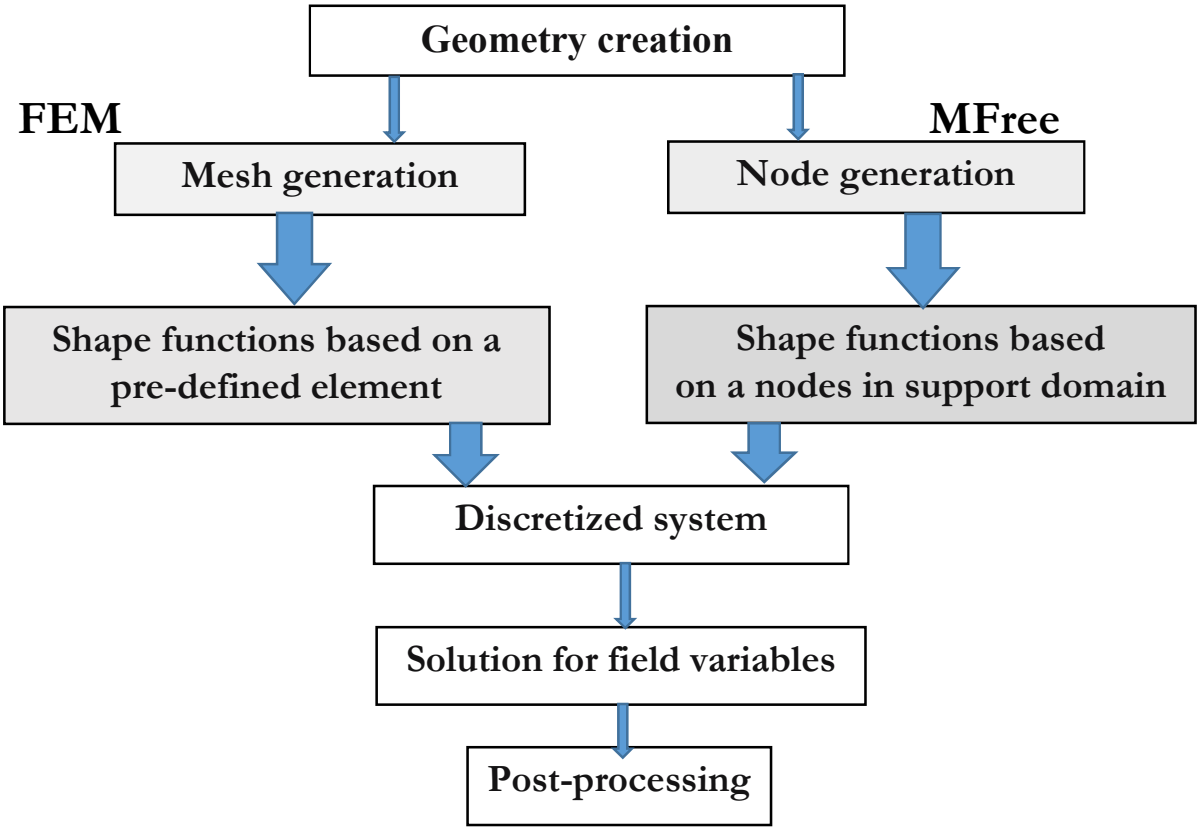

Fig. (2.1) Flow chart for FEM and MFree method

1) The methods depart at the stage of mesh creation.
2) The constructions of the shape functions in these two methods are different. In the finite element method, the shape functions are constructed using predefined elements, and the shape functions are the same for the entire element. In MFree methods, however, the shape functions constructed are usually only for a particular point of interest based on selected local nodes; the shape functions can change when the point of interest changes.
3) The methods follow the similar procedure once the global discretized system equation is established. Therefore, many techniques developed for the FEM can be used in MFree methods.

2.2.2 Steps for MFree method

Step 1: Domain Representation

In the MFree method, the problem domain and its boundary are first modelled and represented by using sets of nodes scattered in the problem domain and on its boundary. Since these nodes carry the values of the field variables in an MFree formulation, they are often called field nodes. The density of the nodes depends on the accuracy required and resources available. The nodal distribution is usually not uniform. Since adaptive algorithms can be used in MFree methods, the density is eventually controlled automatically and adaptively in the code; the initial nodal distribution becomes not important. An MFree method should be able to work for an arbitrary nodal distribution. In the finite element method, this step is different: meshing needs to be performed to discretize the geometry and create the elements. The domain has to be meshed properly into elements of specific shapes such as triangles and quadrilaterals. No overlapping or gaps are allowed. Information, such as the element connectivity, has also to be created during the meshing for later creation of system equations. Mesh generation is a very important part of the pre-process of the finite element method. It is ideal to have an entirely automated mesh generator; unfortunately, it is not practically available for

general situations. Figure (2.2) shows the differences of the domain representation in the MFree method and the FEM.

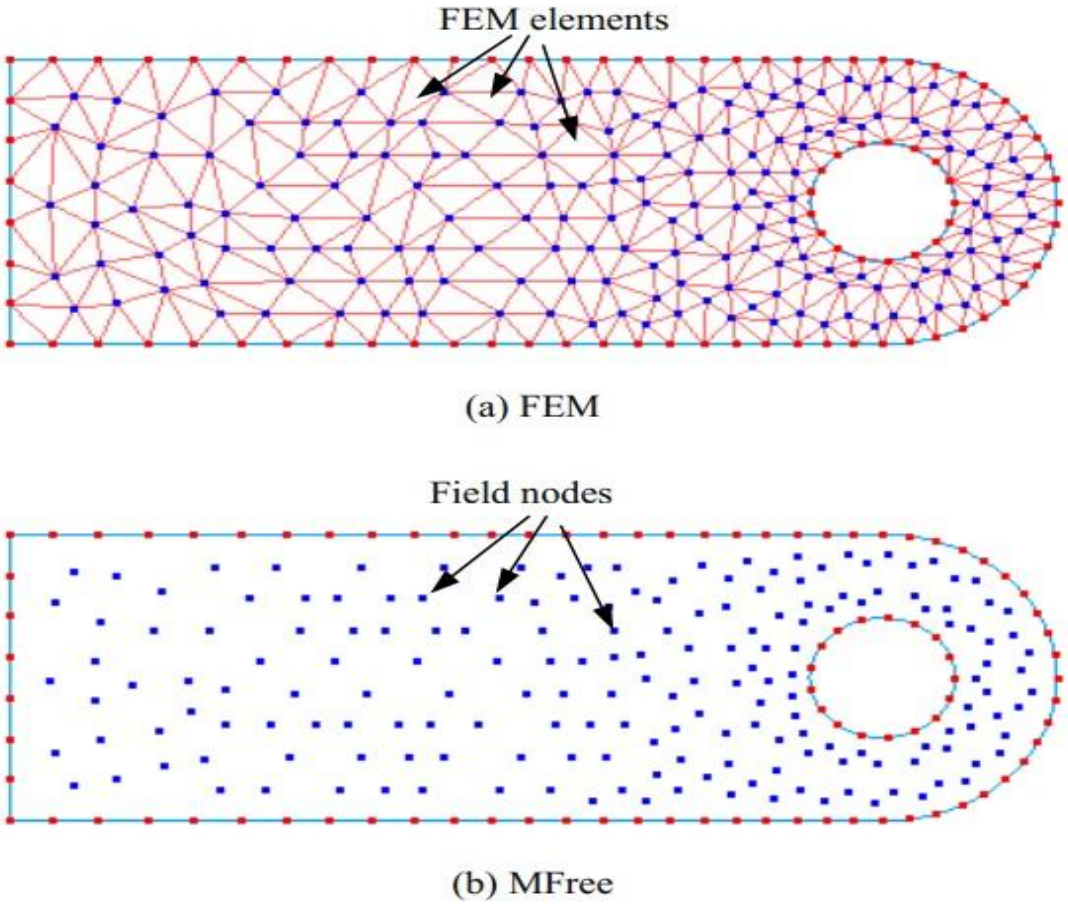

Fig.(2.2) Domain Representation in Fem and MFree

Step 2: Function interpolation/approximation

Since there is no mesh of elements in an MFree method, the field variable (e.g., a component of the displacement) u at any point at $\boldsymbol{x} = (x, y, z)$ within the problem domain is interpolated using function values at field nodes within a small local support domain of the point at $\boldsymbol{x}$, i.e.,

$$\boldsymbol{u(x)} = \sum_{i=1}^{n} \boldsymbol{\psi}_i(x)\boldsymbol{u}_i = \boldsymbol{\psi}^T(x)\, \boldsymbol{U}_s \qquad (1)$$

where n is the number of the nodes that are included in the local support domain of the point at $\boldsymbol{x}$, u_i is the nodal field variable at the ith node, **U**s is the vector that collects all

the field variables at these n nodes, and $\emptyset_i$ is the shape function of the ith node determined using these nodes included in the support domain of $\mathbf{x}$. As the shape functions will not be used regarded as zero outside the local support domain in an MFree method, we often say that the shape functions is locally support. A local support domain of a point $\boldsymbol{x}$ determines the number of nodes to be used to support or approximate the function value at $\boldsymbol{x}$. The support domain can have different shapes and its dimension and shape can be different for different points of interest $\boldsymbol{x}$, as shown in Figure (2.3) they are usually circular or rectangular. In the finite element method, the shape functions are constructed using pre-defined elements. In fact, if the so-called natural coordinate systems are used, the shape functions in the natural coordinates are the same for all the elements of the same type.

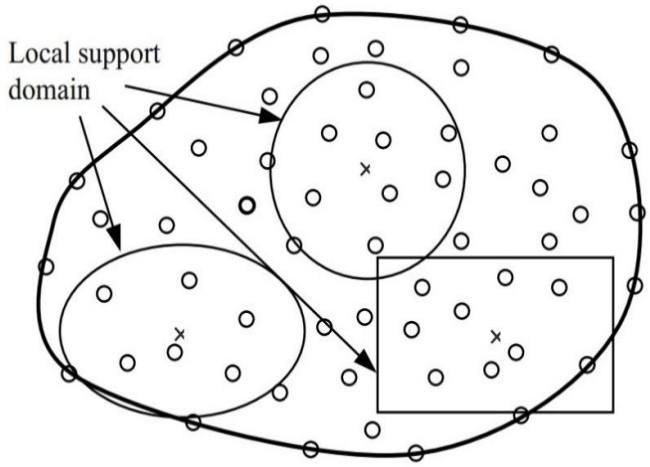

x : point of interest o: field node

Fig. (2.3) Local support domains used in the MFree method to construct shape functions

Step 3: Formation of system equations

The discrete equations of an MFree method can be formulated using the shape functions and strong or weak form system equation. These equations are often written in nodal matrix form and are assembled into the global system matrices for the entire problem domain. The discretized system equations of MFree methods are similar to those of FEM .

Step 4: Solve the global MFree equations

This is similar to that for FEM, except solvers for asymmetric matrix systems may be needed.

2.3 Meshfree Shape Function Construction

MFree shape function are locally supported, because only a set of field nodes in a small local domain are used in the construction and the shape function is not used or regarded as zero outside the local domain. Such a local domain is termed the support domain or influence domain or smoothing domain. In the finite element method (FEM), the shape functions are created using interpolation techniques based on elements formed by a set of fixed nodes. This type of interpolation is termed stationary element based interpolation. In MFree methods, the problem domain is usually represented by field nodes that are, in general, arbitrarily distributed. The field variables at an arbitrary point in the problem domain are approximated using a group of field nodes in a local support domain. Hence, a moving domain based interpolation / approximation technique is necessary to construct the MFree shape function for the approximation of the field variables using a set of arbitrarily distributed nodes. In the development of an MFree method, the construction of efficient MFree shape functions is the foremost issue needed to be settled.

2.3.1 Meshfree interpolation/approximation techniques

A good method for creating MFree shape functions should satisfy some basic requirements.

1) It should be sufficiently robust for reasonably arbitrarily distributed nodes (arbitrary nodal distribution).

2) It should be numerically stable (stability).

3) It should satisfy up to a certain order of consistency (consistency).

4) It should be compactly supported (compact), i.e., it should be regarded as zero outside a bounded region, the support domain.

5) The approximated unknown function using the shape function should be compatible (compatibility) throughout the problem domain when a global weak-form is used, or should be compatible within the local quadrature domain when a local weak-form is used.

6) It is ideal if the shape function possesses the Kronecker delta function property (Delta function property), i.e. the shape function is unit at the node and zero at other nodes in the support domain.

7) It should be computationally efficient (efficiency)

The stability condition concerns two issues. The first is the interpolation stability, meaning that the shape functions constructed should be stable with respect to small perturbations of node locations in the support domain. This requires the moment matrix created using the arbitrarily distributed nodes to be well-conditioned. The second issue is the solution stability, meaning that the numerical solution using the shape functions together with a formulation procedure should not have the so-called numerical or unphysical oscillations. The consistence is important for an accurate function approximation and convergence of the MFree method.

When a global weak form is used, the global compatibility of the shape function, meaning that it has to be compatible in the entire global problem domain, is required. When local weighted residual methods of collocation methods are used for establishing the discretized system equations, only local compatibility in the local weighted domain is required. The Kronecker delta function property is not rigid

because one can use special measures to impose essential boundary conditions if the MFree shape function does not have this property.

2.4 Support Domain

The accuracy of interpolation for the point of interest depends on the nodes in the support domain as shown in Figure (4) below. Therefore, a suitable support domain should be chosen to ensure an efficient and accurate approximation. For a point of interest at X_Q, the dimension of the support domain d_s is determined by

$$\boldsymbol{d_s = \alpha_s d_c} \tag{2}$$

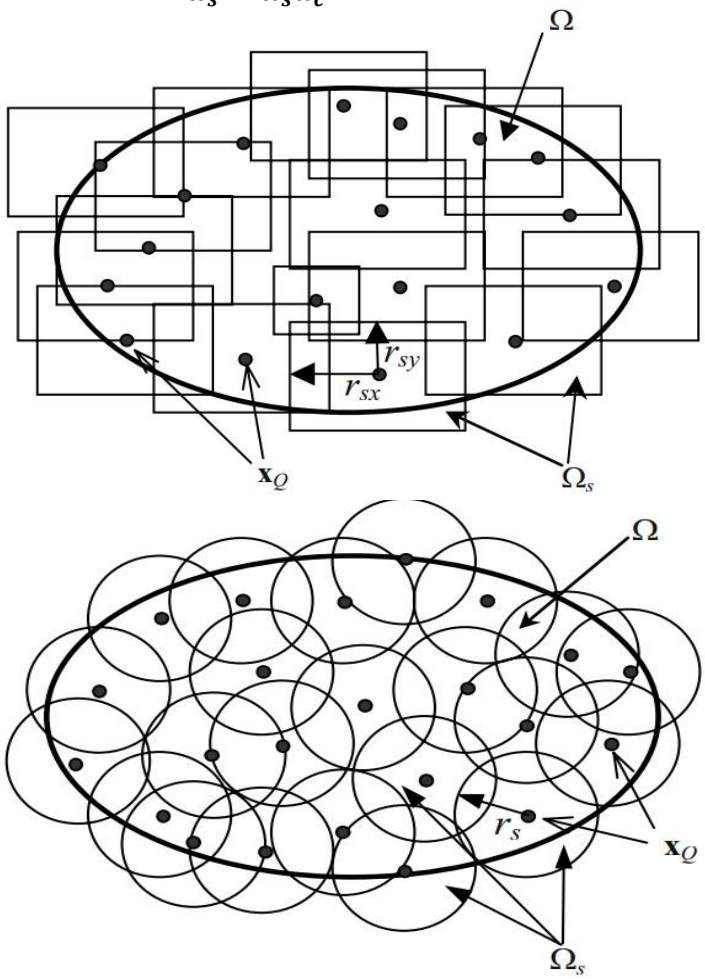

Fig. (2.4) Support domains of points of interest at X_Q in MFree models.(a) Circular support domains (r_s : the dimension of the support domain); (b) rectangular support domains (r_{sx} and r_{sy}: dimensions of the support domain in x and y directions). The support domain is centered by X_Q.

Where α_s is the dimensionless size of the support domain, and $d_c$is is the nodal spacing near the point at X_Q. If the nodes are uniformly distributed, dc is simply the distance between two neighboring nodes. When nodes are non-uniformly distributed, d_c can be defined as an average nodal spacing in the support domain of X_Q. The dimensionless size of the support domain α_s controls the actual dimension of the support domain. For example, α_s =2.1 means a support domain whose radius is 2.1 times the average nodal spacing. The actual number of nodes " n " can be determined by counting all the nodes included in the support domain. Note that α_s should be pre-determined by the analyst before analysis, and it is usually determined by carrying out numerical experiments for a class of benchmark problems for which we already have solutions. Generally, α_s =2.0~3.0 leads to good results for many problems that we have studied.

2.4.1 Determination of the average nodal spacing

For one-dimensional cases, the simplest method of defining an average nodal spacing could be,

$$\boldsymbol{d_{mi} = \frac{D_s}{(n_{Ds}-1)}} \tag{3}$$

Where Ds is an estimated d_{mi} (in Equation (2)) that does not have to be very accurate but should be known and is a reasonably good estimate of d_{mi}, and n_{Ds} is the number of nodes covered by the domain with the dimension of D_s.

For two-dimensional cases, the simplest method of defining an average nodal spacing could be

$$\boldsymbol{d_{mi} = \frac{\sqrt{A_s}}{(\sqrt{n_{A_s}}-1)}} \tag{4}$$

Where A_s is the area of the estimated support domain. The estimate does not have to be accurate, but should be known and should be a reasonably good estimate; n_{A_s} is the number of nodes covered by the estimated domain with the area of As.

Similarly, for three-dimensional cases, the simplest method of defining an average nodal spacing could be

$$\boldsymbol{d_{mi}} = \frac{\sqrt{\boldsymbol{V_s}}}{(\sqrt{\boldsymbol{n_{V_s}}}-\mathbf{1})} \tag{5}$$

where V_s is the volume of the estimated support domain, and n_{V_s} is the number of nodes covered by the estimated domain with the volume of V_s .

we can easily determine the dimension of the support domain d_{mi} for a point at X_Q in a domain with nonuniformly distributed nodes. The procedure is,

1. Estimate d_{mi} for the point at X_Q, which gives D_s or A_s or V_s.
2. Count nodes that are covered by D_s or A_s or V_s, which yields n_{d_s} , n_{A_s} , andn_{V_s}.
3. Use Equation (3) or (4) or (5) to calculate d_c.
4. Calculate d_{mi} using Equation (2), for a given (desired) dimensionless size of support domain.

2.5 Moving Least Squares Shape Functions

The moving least squares (MLS) approximation was devised by mathematicians in data fitting and surface construction (Lancaster and Salkausdas 1981; Cleveland 1993). It can be categorized as a method of series representation of functions. An excellent description of the MLS method can be found in a paper by Lancaster and Salkausdas (1981). The MLS approximation is now widely used in MFree methods for constructing MFree shape functions.

2.5.1 Formulation of MLS shape functions

Consider an unknown scalar function of a field variable $u(x)$ in the domain: The MLS approximation of $u(x)$ is defined at x as,

$$\boldsymbol{u^h(x) = \sum_{j=1}^{m} p_j(x)\, a_j\,(x) = P^T(x)a(x)} \tag{6}$$

Where $P(x)$ is the basis function of the spatial coordinates, $X^T = [x, y]$ for two dimensional problem, and m is the number of the basis functions. The basis function $P(x)$ is often built using monomials from the Pascal triangle to ensure minimum completeness. $a(x)$ is a vector of coefficients given by,

$$\boldsymbol{a^T(x) = \{a_1(x) \quad a_2(x) \quad a_3(x) \ldots\ldots\ldots a_n(x)\}} \tag{7}$$

Note that the coefficient vector $a(x)$ in Equation (7) is a function of x. The coefficients a can be obtained by minimizing the following weighted discrete L2 norm.

$$\boldsymbol{J = \sum_{i=1}^{n} \widehat{W}(x - x_i)\,[P^T(x_i)a(x) - u_i]^2} \tag{8}$$

Where n is the number of nodes in the support domain of x for which the weight function $\widehat{W}(x - x_i) \neq 0$, and u_i is the nodal parameter of u at $x = xi$. Equation (8) is a functional, a weighted residual, that is constructed using the approximated values and the nodal parameters of the unknown field function. Because the number of nodes, n, used in the MLS approximation is usually much larger than the number of unknown coefficients, m, the approximated function, $u^h(x)$, does not pass through the nodal values, as shown in Figure (5).

The stationarity of J with respect to $a(x)$ gives,

$$\boldsymbol{\frac{\partial J}{\partial a} = 0} \tag{9}$$

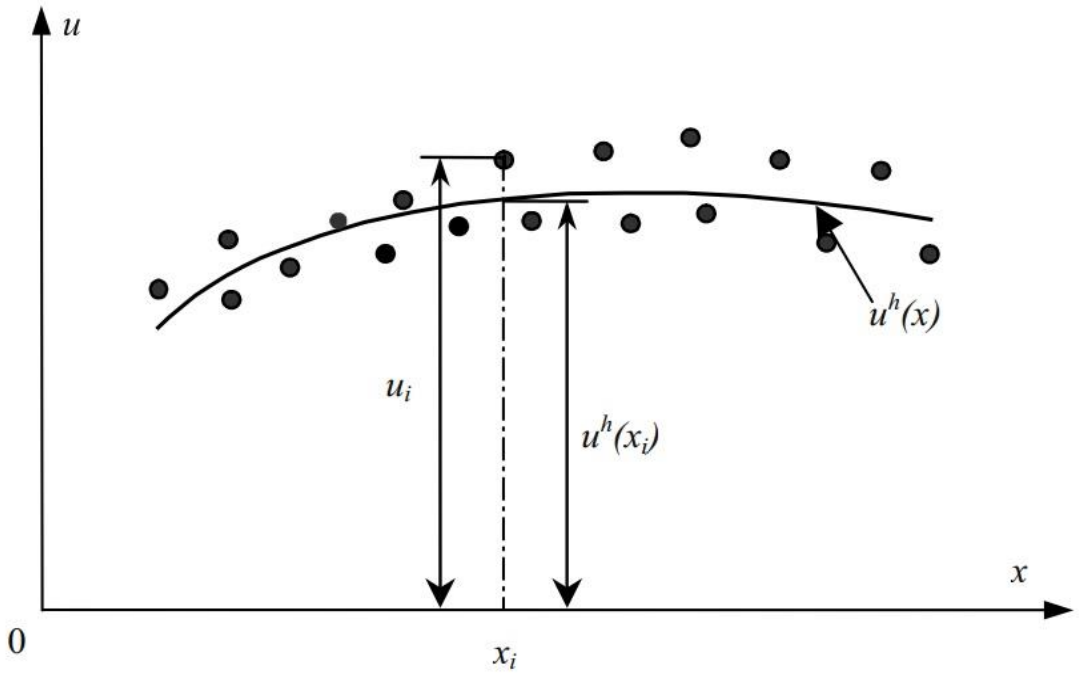

Fig. (2.5)The approximate function $u^h(x)$ and the nodal parameters u_i in the MLS approximation.

Which leads to the following set of linear relations,

$$\boldsymbol{A(x)a(x) = H(x)U_s} \tag{10}$$

Where, U_s is the vector that collects the nodal parameters of field function for all the nodes in the support domain.

$$\boldsymbol{U_s} = \{\boldsymbol{u_1} \quad \boldsymbol{u_2} \ldots\ldots\ldots\ldots \boldsymbol{u_n}\}^T \tag{11}$$

and $A(x)$ is called the weighted moment matrix defined by

$$\boldsymbol{A(x)} = \sum_{i=1}^{n} \widehat{\boldsymbol{W}}_i(\boldsymbol{x})\, \boldsymbol{P(x_i)P^T(x_i)} \tag{12}$$

Where , $\widehat{\boldsymbol{W}}_i(\boldsymbol{x}) = \widehat{\boldsymbol{W}}(\boldsymbol{x} - \boldsymbol{x_i})$

For a two-dimensional problem and using the linear basis (m=3), A is a symmetric 3u3 matrix that can be explicitly written as,

$$\boldsymbol{A_{3\times3}(x) = \sum_{i=1}^{n} \widehat{W}_{\iota}(x)\, P(x_i) P^T(x_i)} \tag{13}$$

$$= \widehat{\boldsymbol{W}}(x - x_1)\begin{bmatrix} 1 & x_1 & y_1 \\ x_1 & {x_1}^2 & x_1 y_1 \\ y_1 & x_1 y_1 & {y_1}^2 \end{bmatrix} + \widehat{\boldsymbol{W}}(x - x_2)\begin{bmatrix} 1 & x_2 & y_1 \\ x_2 & {x_2}^2 & x_2 y_2 \\ y_2 & x_2 y_2 & {y_2}^2 \end{bmatrix} + \ldots\ldots$$

$$. + \widehat{\boldsymbol{W}}(x - x_n)\begin{bmatrix} 1 & x_n & y_n \\ x_n & {x_n}^2 & x_n y_n \\ y_n & x_n y_n & {y_n}^2 \end{bmatrix}$$

$$= \begin{bmatrix} \sum_{i=1}^{n} \widehat{W}_i & \sum_{i=1}^{n} \widehat{W}_i\, x_n & \sum_{i=1}^{n} \widehat{W}_i\, y_n \\ \sum_{i=1}^{n} \widehat{W}_i\, x_n & \sum_{i=1}^{n} \widehat{W}_i\, {x_n}^2 & \sum_{i=1}^{n} \widehat{W}_i\, x_n y_n \\ \sum_{i=1}^{n} \widehat{W}_i\, y_n & \sum_{i=1}^{n} \widehat{W}_i\, x_n y_n & \sum_{i=1}^{n} \widehat{W}_i\, {y_n}^2 \end{bmatrix}_{3\times3} \tag{14}$$

The matrix B in Equation (10) is defined as,

$$\boldsymbol{H(x) = \left[\ \widehat{W_1}(x) P(x_1) \quad \widehat{W_2}(x) P(x_2) \ldots\ldots\ldots\ldots\ldots \widehat{W_n}(x) P(x_n)\ \right]} \tag{15}$$

Which is a $3 \times n$ matrix, and can be expressed explicitly as,

$$= \left[\widehat{\boldsymbol{W}}(x - x_1)\begin{bmatrix} 1 \\ x_1 \\ y_1 \end{bmatrix} + \widehat{\boldsymbol{W}}(x - x_2)\begin{bmatrix} 1 \\ x_2 \\ y_2 \end{bmatrix} + \cdots \ldots\ldots\ldots + \widehat{\boldsymbol{W}}(x - x_n)\begin{bmatrix} 1 \\ x_n \\ y_n \end{bmatrix} \right]$$

$$= \begin{bmatrix} \widehat{W_1} & \widehat{W_2} & \ldots\ldots\ldots\ldots & \widehat{W_n} \\ x_1 \widehat{W_1} & x_2 \widehat{W_2} & \ldots\ldots\ldots\ldots & x_n \widehat{W_n} \\ y_1 \widehat{W_1} & y_2 \widehat{W_2} & \ldots\ldots\ldots\ldots & y_n \widehat{W_n} \end{bmatrix}_{(3\times n)} \tag{16}$$

Solving Equation (10) for $a(x)$, we have

$$\boldsymbol{a\,(x) = A^{-1}\,(x) H\,(x) U_s} \tag{17}$$

Substituting the above equation back into Equation (6), we obtain.

$$\boldsymbol{u^h(x) = \sum_{i=1}^{m} \psi_i(x)\, u_i = \psi^T(x) U_s} \tag{18}$$

Where $\boldsymbol{\psi(x)}$ is the vector of MLS shape functions corresponding n nodes in the support domain of the point$x$, and can be written as,

$$\boldsymbol{\psi^T(x) = \{\psi_1(x)\ \psi_2(x)\ \ldots\ldots\ldots \psi_n(x)\}_{(1\times n)} = \underbrace{P^T(x)}_{1\times 3}\underbrace{A^{-1}(x)}_{3\times 3}\underbrace{H(x)}_{3\times n}} \quad (19)$$

The shape function $\boldsymbol{\psi_i(x)}$ for the i^{th} node is defined by,s

$$\boldsymbol{\psi_i(x) = \sum_{j=1}^{m} p_j\,(A^{-1}(x)\,H(x))_{ji} = P^T(x)(A^{-1}H)_i} \quad (20)$$

In the MLS, the coefficient **a** is the function of x which makes the approximation of weighted least squares move continuously. Therefore, the MLS shape function will be continuous in the entire global domain, as long as the weight functions are chosen properly.

2.6 Choice of the weight function

Equation (20) shows that the continuity of the MLS shape function is governed by the continuity of the basis function p as well as the smoothness of the matrices $\boldsymbol{A}$ and $\boldsymbol{B}$. The latter is governed by the smoothness of the weight function. Therefore, the weight function plays an important role in the performance of the MLS approximation. In the reported studies so far, $\widehat{W}(x - x_i)$ is always chosen to have the following properties.

1) $\widehat{W}(x - x_i) > 0$ within the support domain.
2) $\widehat{W}(x - x_i) = 0$ outside the support domain.
3) $\widehat{W}(x - x_i)$ monotonically decreases from the point of interest at x.
4) $\widehat{W}(x - x_i)$ is sufficient smooth, especially on the boundary of Ω_s.

The last condition is to ensure a smooth inclusion and exclusion of nodes when the support domain moves, so as to guarantee the compatibility of the MLS shape function in the entire problem domain. The choice of the weight function is more or less arbitrary as long as the requirements are met. The exponential function and spline functions are often used in practice.

- **The cubic spline function (W1) has the following form of**

$$\widehat{W}_\iota(x) = \begin{cases} \frac{2}{3} - 4\bar{r}_\iota^{\,2} + 4\bar{r}_\iota^{\,3} & \bar{r}_\iota \le 0.5 \\ \frac{2}{3} - 4\bar{r}_\iota + 4\bar{r}_\iota^{\,2} - \frac{4}{3}\bar{r}_\iota^{\,3} & 0.5 < \bar{r}_\iota \le 1 \\ 0 & \bar{r}_\iota > 1 \end{cases}$$

which has 2nd order continuity (GR Liu and Liu, 2003). (27)

- **The quartic spline function (W2) is given by**

$$\widehat{W}_\iota(x) = \begin{cases} 1 - 6\bar{r}_\iota^{\,2} + 8\bar{r}_\iota^{\,3} - 3\bar{r}_\iota^{\,4} & \bar{r}_\iota \le 1 \\ 0 & \bar{r}_\iota > 1 \end{cases}$$

which has 3rd order continuity (GR Liu and Liu, 2003) (28)

- **The exponential function (W3) is expressed as**

$$\widehat{W}_\iota(x) = \begin{cases} e^{-(\frac{\bar{r}_\iota}{\propto})^2} & \bar{r}_\iota \le 1 \\ 0 & \bar{r}_\iota > 1 \end{cases}$$

2.6.1 Derivatives of weight function and shape function

For the cubic spline weight function is chosen as follows:

$$\mathbf{W(r)} = \begin{cases} \frac{2}{3} - 4\mathbf{r}^2 + 4\mathbf{r}^3 & \text{if } \mathbf{r} \le \frac{1}{2} \\ \frac{4}{3} - 4\mathbf{r} + 4\mathbf{r}^2 - \frac{4}{3}\mathbf{r}^3 & \text{if } \frac{1}{2} < \mathbf{r} \le 1 \\ 0 & \text{if } \mathbf{r} > 1 \end{cases}$$

in which $\mathbf{r} = \|\mathbf{x} - \mathbf{x_i}\| / \mathbf{d_{mi}}$ and $\mathbf{d_{mi}}$ is the size of the domain influence of the $\mathbf{i}$-th node. It may be observed that the first and second derivatives of $\mathbf{W(r)}$ with respect to $\mathbf{x}$ are necessary for computing the derivatives of the matrices $\mathbf{[\Psi]}$, $\mathbf{[A]}$, $\mathbf{[H]}$ and $\mathbf{[B]}$. These derivatives are computed as follows:

$$\frac{dW(r)}{dx}=\begin{cases}(-8r+12r^2)\,\mathrm{sign}(x-x_i)/d_{mi} & \text{if } r\le\frac{1}{2}\\ (-4+8r-4r^2)\,\mathrm{sign}(x-x_i)/d_{mi} & \text{if } \frac{1}{2}<r\le 1\\ 0 & \text{if } r>1\end{cases},$$

$$\frac{d^2W(r)}{dx^2}=\begin{cases}(-8+24r)/(d_{mi})^2 & \text{if } r\le\frac{1}{2} & \text{if } r\le\frac{1}{2}\\ (8-8r)/(d_{mi})^2 & \text{if } \frac{1}{2}<r\le 1 & \text{if } \frac{1}{2}<r\le 1\\ 0 & \text{if } r>1 & \text{if } r>1\end{cases},$$

$$[\psi]_{,x}=\{P\}_{,x}^{T}[A]^{-1}[H]+\{P\}^{T}[A]_{,x}^{-1}[H]+\{P\}^{T}[A]^{-1}[H]_{,x},\ [A]_{,x}^{-1}=-[A]^{-1}[A]_{,x}[A]^{-1},$$

$$[A]_{,x}=\sum_{i=1}^{n}\frac{dW(r)}{dx}\{P_i\}\{P_i\}^{T},\ [A]_{,xx}=\sum_{i=1}^{n}\frac{d^2W(r)}{dx^2}\{P_i\}\{P_i\}^{T},\ \{H_i\}_{,x}=\frac{dW(r)}{dx}\{P_i\},$$

$$\{H_i\}_{,xx}=\frac{d^2W(r)}{dx^2}\{P_i\},\ [A]_{,xx}^{-1}=-[A]_{,x}^{-1}[A]_{,x}[A]^{-1}-[A]^{-1}[A]_{,xx}[A]^{-1}-[A]^{-1}[A]_{,x}[A]_{,x}^{-1},$$

$$\begin{aligned}[\psi]_{,xx}=&\{P\}_{,xx}^{T}[A]^{-1}[H]+2\{P\}_{,x}^{T}[A]_{,x}^{-1}[H]+2\{P\}_{,x}^{T}[A]^{-1}[H]_{,x}+2\{P\}^{T}[A]_{,x}^{-1}[H]_{,x}\\&+\{P\}^{T}[A]_{,xx}^{-1}[H]+\{P\}^{T}[A]^{-1}[H]_{,xx}\end{aligned}$$

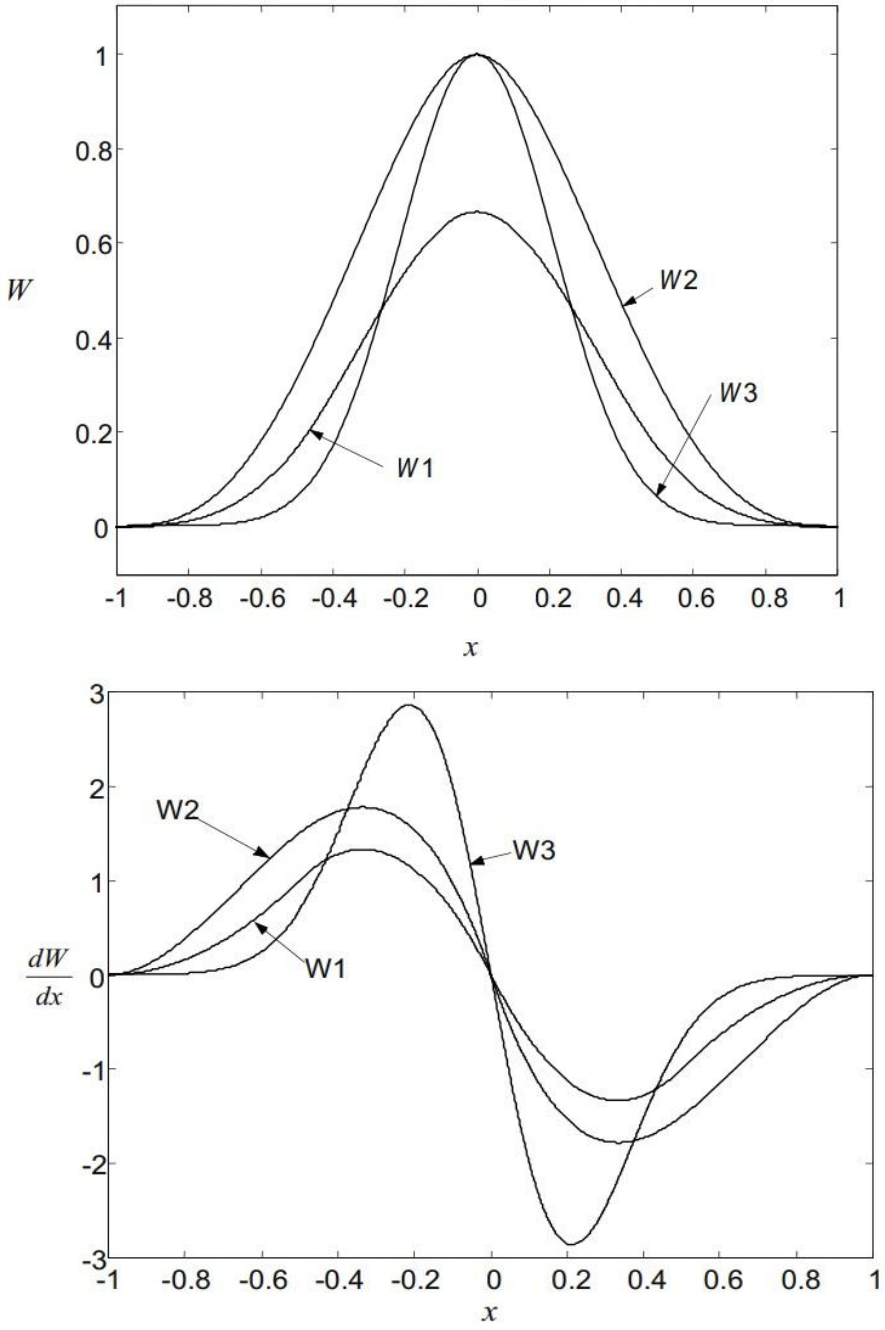

Fig,(2.6) Weight functions and their first order derivatives. W1: cubic spline; W2: quartic spline; W3: exponential function (a) Weight functions; (b) the first order derivatives.

3. ANALYSIS OF SMART COMPOSITE BEAM

A smart structure is made up of a purely elastic material, called the substrate, integrated with distributed actuators and/or sensors. This structure is capable of achieving shape control as soon as it is deformed. These materials induce an electric potential/charge when they are subjected to a mechanical deformation by virtue of the direct piezoelectric effect and are deformed due to the externally applied voltage/charge by virtue of the converse piezoelectric effect. Use of piezoelectric materials as distributed sensors and/or actuators, has been significantly increasing during the past decade for active control of vibration of high performing lightweight smart structures .Use of piezoelectric materials as distributed sensors and actuators is attributed to these two phenomena. When the elastic structure is coupled with a layer/patch of these materials acting as distributed sensors and/or actuators, the resulting structure is known as the smart structure or adaptive structure or smart structure. The main drawback of the existing monolithic piezoelectric materials is that the control Authority of these materials is very low as their piezoelectric stress/strain co-efficients are of very small magnitudes. As the active damping of smart structures depends on the control authority of the piezoelectric materials, tailoring of the piezoelectric stress/strain coefficients may improve their control authority and hence the damping characteristics of lightweight smart structures can be improved.

3.1 Applications of Smart Structure

Conventional mechanical actuation, such as in the shape control of wings, requires various mechanical linkages and joints. In the transportation industry, especially in aerospace, weight is one of the main constraints. Large space structure usually involves precision work and vibration becomes important issue. Thus they too desire to have minimum parts. Smart structures are receiving increasing attention and their numerous applications range from vibration suppression in aircraft

and large space structure; self-diagnostic application for detection of cracks or defects within a structure; Besides vibration control, there is a large number of applications in biomedical, aerospace structure, civil/construction, military, locomotive, flight control and numerous other fields. The smartness of a structure that is enhanced by adaptive materials depends on the control system. Different application such as vibration suppression, buckling control or shape control would require different control algorithms but the overall objective is the same the controller uses the input from the sensors and produces the appropriate actuator output based on control algorithm.

3.1.1 Formulation for Smart Composite Beam Using MFree Method

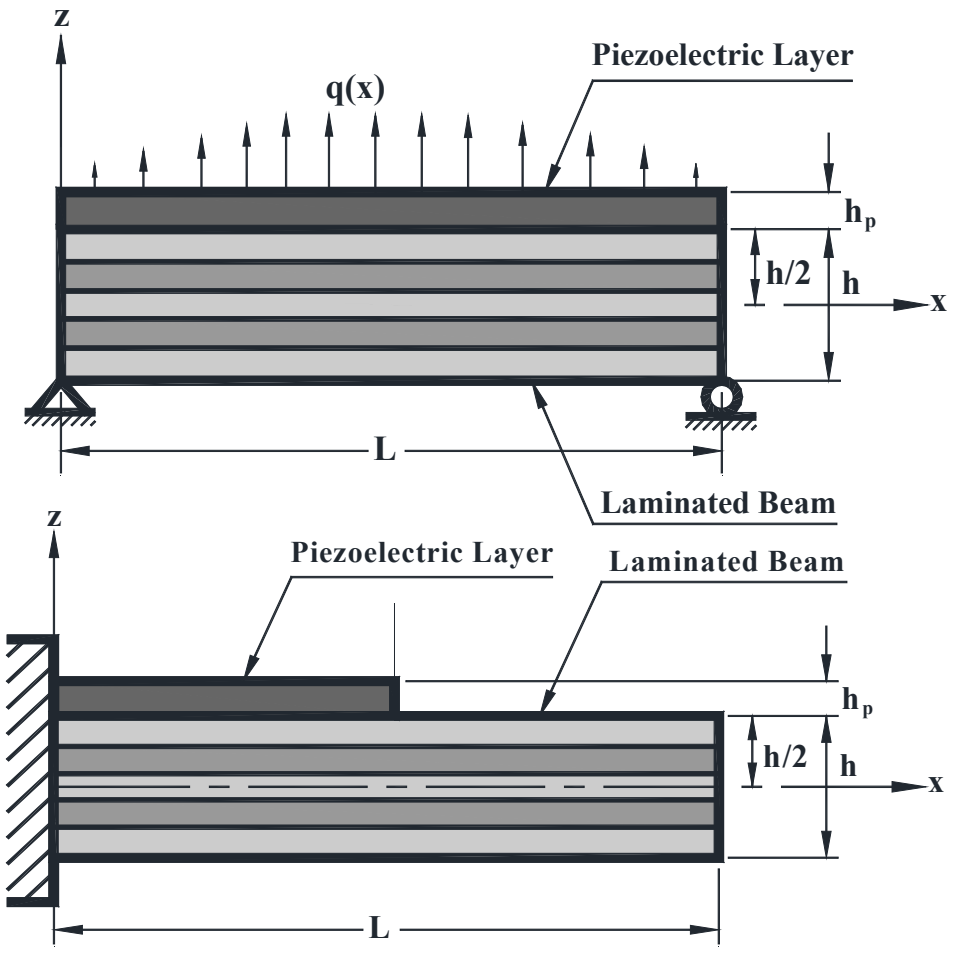

Fig.3.1 Schematic diagrams of smart (a) simply supported and (b) cantilevered laminated composite beams

Figure 3.1 illustrates the schematic diagrams of smart simply supported and cantilevered laminated composite beams. The top surface of the simply supported laminated beam is fully integrated with a piezoelectric layer while the top surface of the cantilevered substrate beam is partially integrated with a patch of the piezoelectric material. The substrate beam is composed of $\mathbf{N}$ number of orthotropic layers. Its length and thickness are denoted by $\mathbf{L}$ and $\mathbf{h}$, respectively while the thickness of the piezoelectric layer is represented by $\mathbf{h_p}$. The top surface of the beam is subjected to a distributed mechanical load $\mathbf{q}(\mathbf{x})$. The piezoelectric layer/patch acts as the distributed actuator of the substrate beams. For actuating the substrate beam, the distributed electric potential (voltage) is applied on the top surface of the piezoelectric layer while the surface of the piezoelectric layer being in contact with the top surface of the substrate beam is grounded. The origin of the coordinate system ($\mathbf{xz}$) is located at one end of the beam such that the lines given by $\mathbf{x = 0}$ and $\mathbf{x = L}$ represent the ends of the beam while the plane given by $\mathbf{z = 0}$ denotes the mid-plane of the substrate beams. The governing stress equilibrium equations and the charge equilibrium equation for an electro-mechanical solid are

$$\boldsymbol{\sigma_{ij,j} = 0} \text{ and } \mathbf{D_{i,i} = 0}\,;\ \mathbf{i, j = x} \text{ and } \mathbf{z} \tag{30}$$

where $\boldsymbol{\sigma_{ij}}$ is the component of Cauchy stress tensor at any point in the solid, $\mathbf{D_i}$ is the electric displacement at the point along the direction denoted by $\mathbf{i}$, $\mathbf{S}$ is the boundary of the solid and $\boldsymbol{\Omega}$ is the volume of the solid. A weak form of the variational principle which would yield the above equilibrium equations is given by

$$\int_S \boldsymbol{\sigma_{ij} n_j \delta u_i dS} + \int_S \mathbf{D_i n_i \delta \phi dS} - \int_\Omega \boldsymbol{\sigma_{ij} \delta \in_{ij}\, d\Omega} - \int_\Omega \mathbf{D_i \delta E_i d\Omega} = \mathbf{0} \tag{31}$$

in which $\boldsymbol{\delta}$ is the symbol of variational operator and executes the first variation of a dependent variable, $\mathbf{u_i}$ and $\mathbf{E_i}$ are the displacements and electric field, respectively at any point in the solid along the direction represented by $\mathbf{i}$, $\boldsymbol{\in_{ij}}$ is the linear strain tensor at the point and $\boldsymbol{\phi}$ is the electric potential. The reduced constitutive relations appropriate for the beam analysis and representing the converse and the direct piezoelectric effects

are given by

$$\{\sigma^p\} = [C^p]\{\in^p\} - [e](E\},$$

(32)

$$\{D\} = [e]^T\{\in^p\} + [\varepsilon](E\} \tag{34}$$

in Eqs. (3) and (4), the state of stresses $\{\sigma^p\}$, the state of strains $\{\in^p\}$, the electric field vector $\{E\}$, the electric displacement vector $\{D\}$, the elastic coefficient matrix $[C^p]$, the piezoelectric constant matrix $[e]$ and the dielectric constant matrix $[\varepsilon]$ are given by

$$\{\sigma^p\} = [\sigma_x^p \quad \sigma_z^p \quad \sigma_{xz}^p]^T,\ \{\in^p\} = [\in_x^p \quad \in_z^p \quad \gamma_{xz}^p]^T,\ \{E\} = [E_x \quad E_z]^T,\ \{D\} = [D_x \quad D_z]^T,$$

$$[C^p] = \begin{bmatrix} C_{11}^p & C_{13}^p & 0 \\ C_{13}^p & C_{33}^p & 0 \\ 0 & 0 & C_{55}^p \end{bmatrix},\ [e] = \begin{bmatrix} 0 & e_{31} \\ 0 & e_{33} \\ 0 & 0 \end{bmatrix} \text{ and } [\varepsilon] = \begin{bmatrix} \varepsilon_{11} & 0 \\ 0 & \varepsilon_{33} \end{bmatrix}$$

(35)

in which, σ_x^p, σ_z^p and σ_{xz}^p are the normal stress along the x-direction, the normal stress along the z-direction and the transverse shear stress, respectively at any point in the piezoelectric layer; while $\in_x^p$, $\in_z^p$ and γ_{xz}^p are the normal strain along the x-direction, the normal strain along the z-direction and the transverse shear strain, respectively at the same point. Also, C_{ij}^p, e_{ij} and ε_{ij} are the elastic coefficients, the piezoelectric coefficients and the dielectric constants of the piezoelectric material, respectively while E_x and E_z are the electric fields along the x-and the z- directions, respectively. The constitutive relations for the k-th orthotropic composite layer of the substrate beam are

$$\{\sigma^k\} = [C^k]\{\in^k\};\ k = 1, 2, 3, \ldots, N \tag{36}$$

The state of stresses $\{\sigma^k\}$, the state of strains $\{\epsilon^k\}$ at any point in the $\mathbf{k}$-th layer of the substrate beam and the elastic coefficient matrix $[\mathbf{C}^k]$ are given by

$$\{\sigma^k\} = [\sigma_x^k \quad \sigma_z^k \quad \sigma_{xz}^k]^T,\ \{\epsilon^k\} = [\epsilon_x^k \quad \epsilon_z^k \quad \gamma_{xz}^k]^T \text{ and } [\mathbf{C}^k] = \begin{bmatrix} \mathbf{C}_{11}^k & \mathbf{C}_{13}^k & \mathbf{0} \\ \mathbf{C}_{13}^k & \mathbf{C}_{33}^k & \mathbf{0} \\ \mathbf{0} & \mathbf{0} & \mathbf{C}_{55}^k \end{bmatrix} \tag{37}$$

in which, σ_x^k, σ_z^k and σ_{xz}^k are the normal stress along the $\mathbf{x}$-direction, the normal stress along the $\mathbf{z}$-direction and the transverse shear stress, respectively at any point in the $\mathbf{k}$-th layer of the substrate beam while ϵ_x, ϵ_z and γ_{xz} are the assumed normal strain along the $\mathbf{x}$-direction, the assumed normal strain along the $\mathbf{z}$-direction and the assumed transverse shear strain, respectively at the same point in the $\mathbf{k}$-th layer. Also, $\mathbf{C}_{ij}^k$ is the elastic constant of the orthotropic $\mathbf{k}$-th layer. It has been proved elsewhere [12] that in case of the piezoelectric layer characterized with large transverse piezoelectric coefficient ($\mathbf{e}_{33}$), the transverse actuation by the piezoelectric layer must be considered and the same equivalent single layer displacement theory cannot be used for both the substrate beam and the actuator layer for accurate analysis of smart structures. Hence, two compatible displacement fields are considered for deriving the present mesh free model (**MFM**) of the smart composite beams. For the substrate beam, an equivalent single layer first order shear deformation theory (F**SDT**) describing the axial displacements $\mathbf{u}$ and $\mathbf{w}$ at any point in the substrate beam along the $\mathbf{x}$ and $\mathbf{z}$ directions, respectively is considered as

$$\mathbf{u} = \mathbf{u_0} + \mathbf{z}\theta_x \text{ and } \mathbf{w} = \mathbf{w_0} + \mathbf{z}\theta_z \tag{38}$$

in which $\mathbf{u_0}$ and $\mathbf{w_0}$ are the translational displacements of any point on the mid-plane ($\mathbf{z}$=0) of the substrate beam along $\mathbf{x}$ and $\mathbf{z}$ directions, respectively; θ_x is the rotation of the normal to the mid-plane of the substrate beam with respect to the $\mathbf{z}$-axis and θ_z is the gradient of the transverse displacement $\mathbf{w}$ with respect to $\mathbf{z}$.

The corresponding axial displacements $\mathbf{u^p}$ and $\mathbf{w^p}$ at any point in the piezoelectric layer are considered as follows:

$$\mathbf{u^p = u_0 + \frac{h}{2}\theta_x + (z - h/2)\gamma_x} \text{ and } \mathbf{w^p = w_0 + \frac{h}{2}\theta_z + (z - h/2)\gamma_z} \tag{39}$$

in which γ_x is the rotation of the transverse normal to the piezoelectric layer across its thickness with respect to the $\mathbf{z}$-axis and γ_z is gradient of the transverse displacement $\mathbf{w^p}$ with respect to the $\mathbf{z}$-axis. The generalized displacement coordinates at any point in the overall beam are expressed in a vector form as follows:

$$\mathbf{\{d\} = [u_0 \quad w_0 \quad \theta_x \quad \theta_z \quad \gamma_x \quad \gamma_z]^T} \tag{40}$$

The variation of electric potential across the thickness of the piezoelectric layer is linear [12]. Thus the electric potential function which is zero at the interface between the piezoelectric layer and the substrate beam may be assumed as

$$\mathbf{\phi(x,z) = \frac{(z - h/2)}{h_p}\phi_0(x)} \tag{41}$$

wherein ϕ_0 is the electric potential distribution at the top surface of the piezoelectric layer. Accordingly, using Eqs. (38)-(41), the states of strains in the substrate beam and the piezoelectric layer and the electric potential field in the piezoelectric layer can expressed as

$$\mathbf{\{\epsilon^k\} = \left[\epsilon_x^k \quad \epsilon_z^k \quad \gamma_{xz}^k\right]^T = \left[\frac{\partial u}{\partial x} \quad \frac{\partial w}{\partial z} \quad \frac{\partial u}{\partial z} + \frac{\partial w}{\partial x}\right]^T = [Z_1]\{\overline{\epsilon}\}},$$

$$\mathbf{\{\epsilon^p\} = \left[\epsilon_x^p \quad \epsilon_z^p \quad \gamma_{xz}^p\right]^T = \left[\frac{\partial u^p}{\partial x} \quad \frac{\partial w^p}{\partial z} \quad \frac{\partial u^p}{\partial z} + \frac{\partial w^p}{\partial x}\right]^T = [Z_2]\{\overline{\epsilon}\}},$$

$$\{\mathbf{E}\} = \begin{bmatrix} \mathbf{E_x} & \mathbf{E_z} \end{bmatrix}^{\mathbf{T}} = -\begin{bmatrix} \frac{\partial \phi}{\partial \mathbf{x}} & \frac{\partial \phi}{\partial \mathbf{z}} \end{bmatrix}^{\mathbf{T}} = [\mathbf{Z_p}]\{\overline{\mathbf{E}}\} \tag{42}$$

In which the matrices $[\mathbf{Z_1}]$, $[\mathbf{Z_2}]$ and $[\mathbf{Z_p}]$, the generalized strain vector $\{\overline{\in}\}$ and the generalized electric field vector $\{\overline{\mathbf{E}}\}$ can be deduced as

$$[\mathbf{Z_1}] = \begin{bmatrix} 1 & 0 & 0 & z & 0 & 0 & 0 & 0 & 0 & 0 \\ 0 & 0 & 0 & 0 & 1 & 0 & 0 & 0 & 0 & 0 \\ 0 & 1 & 1 & 0 & 0 & z & 0 & 0 & 0 & 0 \end{bmatrix}, \quad [\mathbf{Z_2}] = \begin{bmatrix} 1 & 0 & 0 & \frac{h}{2} & 0 & 0 & 0 & z-\frac{h}{2} & 0 & 0 \\ 0 & 0 & 0 & 0 & 1 & 0 & 0 & 0 & 1 & 0 \\ 0 & 1 & 0 & 0 & 0 & \frac{h}{2} & 1 & 0 & 0 & z-\frac{h}{2} \end{bmatrix},$$

$$[\mathbf{Z_p}] = -\begin{bmatrix} \frac{z-h/2}{h_p} & 0 \\ 0 & 1 \end{bmatrix}, \quad \{\overline{\in}\} = [\mathbf{L}]\{\mathbf{d}\}, \quad \{\overline{\mathbf{E}}\} = \{\mathbf{L_p}\}\phi_0,$$

$$[\mathbf{L}]^{\mathbf{T}} = \begin{bmatrix} \frac{\partial}{\partial x} & 0 & 0 & 0 & 0 & 0 & 0 & 0 & 0 & 0 \\ 0 & \frac{\partial}{\partial x} & 0 & 0 & 0 & 0 & 0 & 0 & 0 & 0 \\ 0 & 0 & 1 & \frac{\partial}{\partial x} & 0 & 0 & 0 & 0 & 0 & 0 \\ 0 & 0 & 0 & 0 & 1 & \frac{\partial}{\partial x} & 0 & 0 & 0 & 0 \\ 0 & 0 & 0 & 0 & 0 & 0 & 1 & \frac{\partial}{\partial x} & 0 & 0 \\ 0 & 0 & 0 & 0 & 0 & 0 & 0 & 0 & 1 & \frac{\partial}{\partial x} \end{bmatrix} \text{ and } \{\mathbf{L_p}\} = \begin{bmatrix} \frac{\partial}{\partial x} & \frac{1}{h_p} \end{bmatrix}^{\mathbf{T}} \tag{43}$$

Utilizing Eqs. (33), (34) and (42), the weak form of the variational principle given by Eq. (32) can be written for the present overall smart composite beams as follows:

$$
\begin{aligned}
&\mathbf{N_x}\delta\mathbf{u_0}\big|_{x=0}+\mathbf{N_x}\delta\mathbf{u_0}\big|_{x=L}+\mathbf{M_x}\delta\theta_x\big|_{x=0}+\mathbf{M_x}\delta\theta_x\big|_{x=L}+\mathbf{M_x^p}\delta\gamma_x\big|_{x=0}\\
&+\mathbf{M_x^p}\delta\gamma_x\big|_{x=L}+\mathbf{Q_x}\delta\mathbf{w_0}\big|_{x=0}+\mathbf{Q_x}\delta\mathbf{w_0}\big|_{x=L}+\mathbf{R_x}\delta\theta_z\big|_{x=0}+\mathbf{R_x}\delta\theta_z\big|_{x=L}+\mathbf{R_x^p}\delta\gamma_z\big|_{x=0}\\
&+\mathbf{R_x^p}\delta\gamma_z\big|_{x=L}+\sum_{k=1}^{N-1}\int_0^L\Big[(\sigma_{xz}^k-\sigma_{xz}^{k+1})\delta\mathbf{u}\big|_{z=h_{k+1}}+(\sigma_z^k-\sigma_z^{k+1})\delta\mathbf{w}\big|_{z=h_{k+1}}\Big]\mathbf{dx}+\\
&\int_0^L\Big[(\sigma_{xz}^N-\sigma_{xz}^p)\delta\mathbf{u}\big|_{z=h/2}+(\sigma_z^N-\sigma_z^p)\delta\mathbf{w}\big|_{z=h/2}\Big]\mathbf{dx}+\int_0^L\Big[(\sigma_{xz}^1\delta\mathbf{u}\big|_{z=-h/2}+\sigma_{xz}^p\delta\mathbf{u}\big|_{z=h/2+h_p}\Big]\mathbf{dx}\\
&+\int_0^L\Big[(\sigma_z^1\delta\mathbf{w}\big|_{z=-h/2}+\sigma_z^p\delta\mathbf{w}\big|_{z=h/2+h_p}\Big]\mathbf{dx}+\overline{\mathbf{D}}_x\delta\phi_0\big|_{x=0}+\overline{\mathbf{D}}_x\delta\phi_0\big|_{x=L}-\int_0^L\delta\{\overline{\in}\}^T[\mathbf{D}]\{\overline{\in}\}\mathbf{dx}\\
&+\int_0^L\delta\{\overline{\in}\}^T[\mathbf{D_{d\phi}}]\{\overline{\mathbf{E}}\}\mathbf{dx}-\int_0^L\delta\{\overline{\mathbf{E}}\}^T[\mathbf{D_{d\phi}}]^T\{\overline{\in}\}\mathbf{dx}-\int_0^L\delta\{\overline{\mathbf{E}}\}^T[\mathbf{D_{\phi\phi}}]^T\{\overline{\mathbf{E}}\}\mathbf{dx}\\
&+\int_0^L\mathbf{D_z}\delta\phi_0\big|_{z=h/2+h_p}\mathbf{dx}+\int_0^L\mathbf{q(x)}[0\quad 1\quad 0\quad h/2\quad 0\quad h_p]\delta\{\mathbf{d}\}\,\mathbf{dx}=0
\end{aligned}
\tag{44}
$$

where

$$
\mathbf{N_x}=\sum_{k=1}^{N}\int_{h_k}^{h_{k+1}}\sigma_x^k\,\mathbf{dz}+\int_{h/2}^{h/2+h_p}\sigma_x^p\,\mathbf{dz},\ \mathbf{M_x}=\sum_{k=1}^{N}\int_{h_k}^{h_{k+1}}\sigma_x^k z\,\mathbf{dz}+\int_{h/2}^{h/2+h_p}\sigma_x^p z\,\mathbf{dz},
$$

$$
\mathbf{M_x^p}=\int_{h/2}^{h/2+h_p}\sigma_x^p(z-h/2)\,\mathbf{dz},\ \mathbf{Q_x}=\sum_{k=1}^{N}\int_{h_k}^{h_{k+1}}\sigma_{xz}^k\,\mathbf{dz}+\int_{h/2}^{h/2+h_p}\sigma_{xz}^p\,\mathbf{dz},
$$

$$
\mathbf{R_x}=\sum_{k=1}^{N}\int_{h_k}^{h_{k+1}}\sigma_{xz}^k\,z\mathbf{dz}+\int_{h/2}^{h/2+h_p}\frac{\mathbf{h}}{2}\sigma_{xz}^p\,\mathbf{dz},\ \mathbf{R_x^p}=\int_{h/2}^{h/2+h_p}\sigma_{xz}^p(z-h/2)\,\mathbf{dz},
$$

$$
\overline{\mathbf{D}}_x=\int_{h/2}^{h/2+h_p}\mathbf{D_x}\frac{(z-h/2)}{\mathbf{h_p}}\mathbf{dz},\ [\mathbf{D_{xx}}]=[\mathbf{D_1}]+[\mathbf{D_2}],
$$

$$
[\mathbf{D_1}]=\sum_{k=1}^{N}\int_{h_k}^{h_{k+1}}[\mathbf{Z_1}]^T[\mathbf{C^k}][\mathbf{Z_1}]\,\mathbf{dz},\ [\mathbf{D_2}]=\int_{h/2}^{h/2+h_p}[\mathbf{Z_2}]^T[\mathbf{C^p}][\mathbf{Z_2}]\,\mathbf{dz},
$$

$$
[\mathbf{D_{x\phi}}]=\int_{h/2}^{h/2+h_p}[\mathbf{Z_2}]^T[\mathbf{e}][\mathbf{Z_p}]\,\mathbf{dz}\ \text{and}\ [\mathbf{D_{\phi\phi}}]=\int_{h/2}^{h/2+h_p}[\mathbf{Z_p}]^T[\varepsilon][\mathbf{Z_p}]\,\mathbf{dz}
\tag{45}
$$

It is to be noted that the z coordinates of the top and bottom surfaces of the k-th layer of the substrate beam are denoted by h_{k+1} and h_k, respectively. In order that the left hand side of Eq. (45) becomes zero, the essential boundary conditions of the present overall smart beams can be derived from the variational principle given by Eq. (44) as follows:

simply supported smart beams:

$$\{d_b\}\big|_{x=0} = [u_0 \quad w_0 \quad \theta_z \quad \gamma_z]^T\Big|_{x=0} = [0 \quad 0 \quad 0 \quad 0]^T \text{ and } \phi_0(0) = 0$$

$$\{d_b\}\big|_{x=L} = [w_0 \quad \theta_z \quad \gamma_z]^T\Big|_{x=L} = [0 \quad 0 \quad 0]^T \text{ and } \phi_0(L) = 0 \tag{46}$$

Clamped-free smart beams:

$$\{d_b\}\big|_{x=0} = [u_0 \quad w_0 \quad \theta_x \quad \gamma_x \quad \theta_z \quad \gamma_z]^T\Big|_{x=0} = [0 \quad 0 \quad 0 \quad 0 \quad 0 \quad 0]^T \tag{47}$$

The variational principle also yields the following interface continuity conditions and prescribed boundary conditions:

$$\sigma_{xz}^k(x, h_{k+1}) = \sigma_{xz}^{k+1}(x, h_{k+1}),\ \sigma_z^k(x, h_{k+1}) = \sigma_z^{k+1}(x, h_{k+1});\ k = 1, 2, 3, \ldots, N-1,$$

$$\sigma_{xz}^N(x, h_{N+1}) = \sigma_{xz}^p(x, h_{N+1}),\ \sigma_z^N(x, h_{N+1}) = \sigma_z^p(x, h_{N+1})$$

$$\sigma_z^1(x, -h/2) = \sigma_{xz}^1(x, -h/2) = 0 \text{ and } \sigma_{xz}^p(x, h/2 + h_p) = 0 \tag{48}$$

4. ELEMENT FREE GALERKIN METHOD

The element-free Galerkin (EFG) method is a meshless method uses the moving least squares (MLS) shape functions, Because the MLS approximation lacks the Kronecker delta function property, the constrained Galerkin weak-form should be posed as follows. The element-free Galerkin (EFG) method is a meshless method because only a set of nodes and a description of the model's boundary are required to generate the discrete equations. The connectivity between the nodes and the approximation functions are completely constructed by the method. The EFG method employs moving least-square (MLS) approximants to approximate the function $u(x)$ with $u^h(x)$. These approximants are constructed from three components: a weight function of compact support associated with each node, a basis, usually consisting of a polynomial, and a set of coefficients that depend on position.

The weight function is nonzero only over a small sub domain around a node, which is called its support. The support of the weight function defines a node's domain of influence, which is the sub domain over which a particular node con tributes to the approximation. The overlap of the nodal domains of influence defines the nodal connectivity. One attractive property of MLS approximations is that their continuity is related to the continuity of the weight function: if the continuity of the basis is greater than the continuity of the weight function, the resulting approximation will inherit the continuity of the weight function. Therefore, a low order polynomial basis, e.g., a linear basis, may be used to generate highly continuous approximations by choosing an appropriate weight function. Thus, post processing to generate smooth stress and strain fields which is required for C^0 finite element methods is unnecessary in EFG. Although EFG is considered meshless when referring to shape function construction or function approximation, a mesh will be required for solving partial differential equations

(PDE's) by the Galerkin approximation procedure. In order to compute the integrals in the weak form, either a regular background mesh or a background cell structure is used.

4.1 Element Free Galerkin Method for Smart Model

The element free Galerkin method is implemented to derive the smart mesh free model (**MFM**). Any generalized displacement say $\mathbf{u_0}$ at any point ($\mathbf{x}$) can be approximated by the moving least squares (**MLS**) approximation as

$$\mathbf{u_0} = \{\mathbf{P}\}^{\mathbf{T}}\{\mathbf{a}\} \tag{49}$$

where $\{\mathbf{P}\}$ is a column vector constructed from a basis function and $\{\mathbf{a}\}$ is a column vector of coefficients of the basis function. The linear basis function for one dimensional problem is considered here. Thus

$$\{\mathbf{P}\} = [\mathbf{1} \quad \mathbf{x}]^{\mathbf{T}} \text{ and } \{\mathbf{a}\} = [\mathbf{a_0(x)} \quad \mathbf{a_1(x)}]^{\mathbf{T}} \tag{50}$$

To determine the vector $\{\mathbf{a}\}$, the domain of influence of any point ($\mathbf{x}$) is considered to contain '$\mathbf{n}$' number of nodes. Considering the length of the beam as the domain of influence of any point ($\mathbf{x}$), the vector $\{\mathbf{a}\}$ is determined by minimizing the following weighted discrete norm:

$$\mathbf{J} = \sum_{\mathbf{i=1}}^{\mathbf{n}} \mathbf{W(x - x_i)}(\{\mathbf{P_i}\}^{\mathbf{T}}\{\mathbf{a}\} - \mathbf{u_{0i}})^{\mathbf{2}} \tag{51}$$

where $\mathbf{x_i}$ is the $\mathbf{x}$-coordinate of the $\mathbf{i}$-th node, $\mathbf{W(x - x_i)}$ is the weight function associated with the $\mathbf{i}$-th node, $\mathbf{u_{0i}}$ is the nodal parameter corresponding to $\mathbf{u_0}$ at the $\mathbf{i}$-th node and $\{\mathbf{P_i}\} = [\mathbf{1} \quad \mathbf{x_i}]^{\mathbf{T}}$. For minimization of $\mathbf{J}$, $\partial \mathbf{J} / \partial \{\mathbf{a}\}$ is set to zero and the following set of equations are obtained:

$$[\mathbf{A}]\{\mathbf{a}\} = [\mathbf{H}]\{\mathbf{d_0}\} \tag{52}$$

in which

$$\{\mathbf{d}_0\} = [\mathbf{u}_{01} \quad \mathbf{u}_{02} \quad \mathbf{u}_{03} \quad . \quad . \quad . \quad . \quad \mathbf{u}_{0n}]^T, \; [\mathbf{A}] = \sum_{i=1}^{n} \mathbf{W}(\mathbf{x}-\mathbf{x}_i)\{\mathbf{P}_i\}\{\mathbf{P}_i\}^T,$$

$$[\mathbf{H}] = \left[\mathbf{W}(\mathbf{x}-\mathbf{x}_i)\{\mathbf{P}_1\} \quad \mathbf{W}(\mathbf{x}-\mathbf{x}_i)\{\mathbf{P}_2\} \quad \mathbf{W}(\mathbf{x}-\mathbf{x}_i)\{\mathbf{P}_3\} \quad . \quad . \quad . \quad . \quad \mathbf{W}(\mathbf{x}-\mathbf{x}_i)\{\mathbf{P}_n\}\right] \quad (53)$$

Substituting for $\{\mathbf{a}\}$ from Eq. (51) into Eq. (48), the approximation of $\mathbf{u_0(x)}$ at any point can be expressed in terms of the nodal parameters of $\mathbf{u_0(x)}$ as

$$\mathbf{u_0} = [\Psi]\{\mathbf{d}_0\} \quad (54)$$

in which

$$[\Psi] = [\psi_1 \quad \psi_2 \quad \psi_3 \quad . \quad . \quad . \quad . \quad \psi_n]^T = \{\mathbf{P}\}^T[\mathbf{A}]^{-1}[\mathbf{H}]$$

with ψ_i being the shape function associated with the $\mathbf{i}$-th node. It is evident that the **MLS** approximations of other generalized displacement variables given by Eq. (50) yields the same shape functions associated with the $\mathbf{i}$-th node. Thus the generalized displacement vector $\{\mathbf{d}\}$ and the electric potential ϕ_0 at any point can be expressed in terms of the nodal generalized displacement parameter vector and the nodal electric potential vector, respectively as follows:

$$\{\mathbf{d}\} = [\mathbf{N}]\{\mathbf{X}\} \text{ and } \phi_0 = [\Psi]\{\Phi\} \quad (55)$$

in which

$$[\mathbf{N}] = \left[[\mathbf{N}_1] \quad [\mathbf{N}_2] \quad [\mathbf{N}_3] \quad . \quad . \quad . \quad . \quad [\mathbf{N}_n]\right],$$

$$\{\mathbf{X}\} = \left[\{\mathbf{d}_1\}^T \quad \{\mathbf{d}_2\}^T \quad \{\mathbf{d}_3\}^T \quad . \quad . \quad . \quad . \quad \{\mathbf{d}_n\}^T\right]^T,$$

$$\{\mathbf{d}_i\} = [\mathbf{u}_{0i} \quad \mathbf{w}_{0i} \quad \theta_{xi} \quad \theta_{zi} \quad \gamma_{xi} \quad \gamma_{zi}]^T, \; [\mathbf{N}_i] = \psi_i \mathbf{I}, \; \mathbf{i} = 1, 2, 3, \ldots, \mathbf{N},$$

$$\{\Phi\} = [\phi_1 \quad \phi_2 \quad \phi_3 \quad . \quad . \quad . \quad . \quad \phi_n]^T \tag{56}$$

Also in Eq. (56), $\mathbf{I}$ is a 6×6 identity matrix and ϕ_i is the nodal electric potential parameter at the $\mathbf{i}$-th node. Using Eqs. (25), the generalized strain vector and the generalized electric field vector can be expressed in terms of the nodal generalized displacement parameter vector and the nodal electric potential vector as follows:

$$\{\overline{\epsilon}\} = [\mathbf{B}]\{\mathbf{X}\} \text{ and } \{\overline{\mathbf{E}}\} = [\mathbf{B}_\phi]\{\Phi\} \tag{57}$$

in which

$$[\mathbf{B}] = [\mathbf{L}][\mathbf{N}] \text{ and } [\mathbf{B}_\phi] = [\mathbf{L}_p][\Psi] \tag{58}$$

Since the mesh free shape function does not satisfy the property of the Kronecker delta function, the essential boundary conditions are satisfied using Lagrange multipliers. Also, electric potential at the top surface of the piezoelectric layer will be prescribed. Accordingly, $\delta\phi_0 = 0$ and using Eqs. (55) and (58), the variational principle given by Eq. (54) can be augmented in terms of the nodal generalized parameters as follows:

$$\begin{aligned}
&\int_0^L \delta\{X\}^T \Big([B]^T[D_{xx}][B]\{X\} - [B]^T[D_{x\phi}][B_\phi]\{\Phi\} - [N]^T[0 \quad 1 \quad 0 \quad h/2 \quad 0 \quad h_p]^T q(x)\Big)dx \\
&+ \delta\{\lambda_0\}^T[U_1][N]\Big|_{x=0}\{X\} + \delta\{\lambda_L\}^T[U_2][N]\Big|_{x=L}\{X\} + \delta\{X\}^T[N]^T[U_1]^T\Big|_{x=0}\{\lambda_0\} \\
&+ \delta\{X\}^T[N]^T[U_2]^T\Big|_{x=L}\{\lambda_L\} - \delta\{\lambda_0\}^T\{d_b\}\Big|_{x=0} - \delta\{\lambda_L\}^T\{d_b\}\Big|_{x=L} - \delta\{X\}^T[N]^T[U_3]^T M_x\Big|_{x=0} \\
&- \delta\{X\}^T[N]^T[U_3]^T M_x\Big|_{x=L} - \delta\{X\}^T[N]^T[U_4]^T M_x^p\Big|_{x=0} - \delta\{X\}^T[N]^T[U_4]^T M_x^p\Big|_{x=L} = 0
\end{aligned} \tag{59}$$

in which $\{\lambda_0\}$ and $\{\lambda_L\}$ are the vectors of Lagrange multipliers for the essential displacement boundary conditions at $\mathbf{x}$=0 and $\mathbf{L}$, respectively. The moment resultants

$\mathbf{M_x}$ and $\mathbf{M_x^p}$, and the various other matrices appearing in Eq. (59) are given by

$$\mathbf{M_x} = [\mathbf{D_3}][\mathbf{B}]\{\mathbf{X}\},\ \mathbf{M_x^p} = [\mathbf{D_4}][\mathbf{B}]\{\mathbf{X}\},$$

$$[\mathbf{D_3}] = \sum_{k=1}^{N} \int_{h_k}^{h_{k+1}} \mathbf{z}[\mathbf{C_{11}^k} \quad \mathbf{C_{13}^k} \quad \mathbf{0}][\mathbf{Z_1}]\mathbf{dz} + \int_{h/2}^{h/2+h_p} (\mathbf{h/2})[\mathbf{C_{11}^p} \quad \mathbf{C_{13}^p} \quad \mathbf{0}][\mathbf{Z_2}]\mathbf{dz},$$

$$[\mathbf{D_4}] = \int_{h/2}^{h/2+h_p} (\mathbf{z-h/2})[\mathbf{C_{11}^p} \quad \mathbf{C_{13}^p} \quad \mathbf{0}][\mathbf{Z_2}]\mathbf{dz},\ [\mathbf{U_1}] = \begin{bmatrix} 1 & 0 & 0 & 0 & 0 & 0 \\ 0 & 1 & 0 & 0 & 0 & 0 \\ 0 & 0 & 0 & 1 & 0 & 0 \\ 0 & 0 & 0 & 0 & 0 & 1 \end{bmatrix},$$

$$[\mathbf{U_2}] = \begin{bmatrix} 0 & 1 & 0 & 0 & 0 & 0 \\ 0 & 0 & 0 & 1 & 0 & 0 \\ 0 & 0 & 0 & 0 & 0 & 1 \end{bmatrix},\ [\mathbf{U_3}] = [0 \quad 0 \quad 1 \quad 0 \quad 0 \quad 0]$$

and $[\mathbf{U_4}] = [0 \quad 0 \quad 0 \quad 0 \quad 1 \quad 0]$ (60)

In order that the left hand side of Eq. (59) be zero, the following discrete governing equations of the overall smart composite beams can be derived:

$$[\mathbf{K}]\{\mathbf{X}\} + [\mathbf{G}]\{\lambda\} = [\mathbf{F_p}]\{\Phi\} + \{\mathbf{F}\} \text{ and } [\mathbf{G}]^{\mathbf{T}}\{\mathbf{X}\} = \{\mathbf{X_b}\} \tag{61}$$

in which the overall stiffness matrix $[\mathbf{K}]$, the matrix $[\mathbf{G}]$, the electro-elastic coupling matrix $[\mathbf{F_p}]$, the mechanical load vector $\{\mathbf{F}\}$, the Lagrange multiplier vector $\{\lambda\}$ and the vector of essential displacement boundary conditions $\{\mathbf{X_b}\}$ are given by

$$[\mathbf{K}] = \int_0^L [\mathbf{B}]^{\mathbf{T}}[\mathbf{D}][\mathbf{B}]\{\mathbf{X}\}\mathbf{dx} - [\mathbf{N}]^{\mathbf{T}}([\mathbf{U_3}]^{\mathbf{T}}[\mathbf{D_3}] + [\mathbf{U_4}]^{\mathbf{T}}[\mathbf{D_4}])[\mathbf{B}]\Big|_{x=0} - [\mathbf{N}]^{\mathbf{T}}([\mathbf{U_3}]^{\mathbf{T}}[\mathbf{D_3}] + [\mathbf{U_4}]^{\mathbf{T}}[\mathbf{D_4}])[\mathbf{B}]\Big|_{x=L},$$

$$\{F\} = \int_0^L [N]^T [0 \quad 0 \quad 0 \quad h/2 \quad 0 \quad h_p]^T \, dx \, , \; [F_p] = \int_0^L [B]^T [D_{x\phi}][B_\phi] dx$$

$$[G] = \begin{bmatrix} [U_1][N]\big|_{x=0} \\ [U_2][N]\big|_{x=L} \end{bmatrix}^T \, , \; \{\lambda\} = [\{\lambda_0\}^T \quad \{\lambda_L\}^T]^T \text{ and } \{X_b\} = [\{d_b\}^T\big|_{x=0} \quad \{d_b\}^T\big|_{x=L}]^T \tag{62}$$

The sets of discrete governing equations given by Eq. (31) represent the mesh free model (MFM of the overall smart composite beams being studied here.

4.2 Computation of axial and transverse shear stresses

Once the nodal generalized parameters are computed by solving Eq. (31), the constitutive relation can be used to compute the axial stress σ_x^k at any point in the k-th layer of the substrate beam as follows:

$$\sigma_x^k = [C_{11}^k \quad C_{13}^k \quad 0][Z_1][B]\{X\} \tag{33}$$

In order to satisfy the continuity conditions at the interface between the adjacent layers and the zero surface shear traction at the top and bottom surface of the overall beam, the transverse shear stress σ_{xz}^k at any point in the k-th layer of the substrate beam cannot be computed using the constitutive relation. However, using Eq. (33) in the governing equilibrium equation given by Eq. (1), the transverse shear stress at any point in the k-th layer of the substrate beam can be computed as follows:

$$\sigma_{xz}^k = -[C_{11}^k \quad C_{13}^k \quad 0][Z_1][B]_{,x}\{X\} + C_k \tag{34}$$

where the constants C_k are determined by satisfying the interface continuity conditions and the surface traction at the bottom surface of the beam.

5. NUMERICAL RESULTS AND DISCUSSIONS

The following material properties for the layers of the substrates are considered for evaluating the numerical results:

$$E_1 = 172.5 \times 10^9;\ E_2 = \frac{E_1}{25}; E_3 = E_2;$$

$$G_{12} = 0.5\ \times\ E_2; G_{12} = G_{23}; G_{12} = 0.2\ \times\ 10^2;$$

$$\mu_{12} = 0.25; \mu_{13} = 0.25; \mu_{23} = 0.25;$$

The results are evaluated with and without applying the electrical potential distribution on the actuator surface for different values of length to thickness ratios s(=a/h) and m=n=1 in the definition of p and q. The following non-dimensional parameters are used for presenting the numerical results.

$$\mathbf{w^* = \frac{100E_T h^3}{q_0 a^4} w(x,0)}$$

$\mathbf{s}$ =50, $\mathbf{h_p}$ =250 μ m, h=0.005m

A program was made in MATLAB to calculate axial stresses and shear stresses across the thickness for three layer composite beam and four layer composite beam. The results are as shown in figure. stresses in the cross-ply substrates (0-90-0) and cross ply (0-90-0-90) are computed with and without applying the externally applied voltage to the piezo layer. These results are shown in Figs. 5.1-5.6 for s -50.The distribution of implies that the top and bottom layers of the substrate undergo bending mainly when V - 0. Due to the combined action of actuator and mechanical loading, these layers also undergo bending predominantly but in a reverse way when V = 100.

5.1 Comparison of Responses of Mfree Method for Three Layered (0/90/0) Composite Beam with Exact Solution Method.

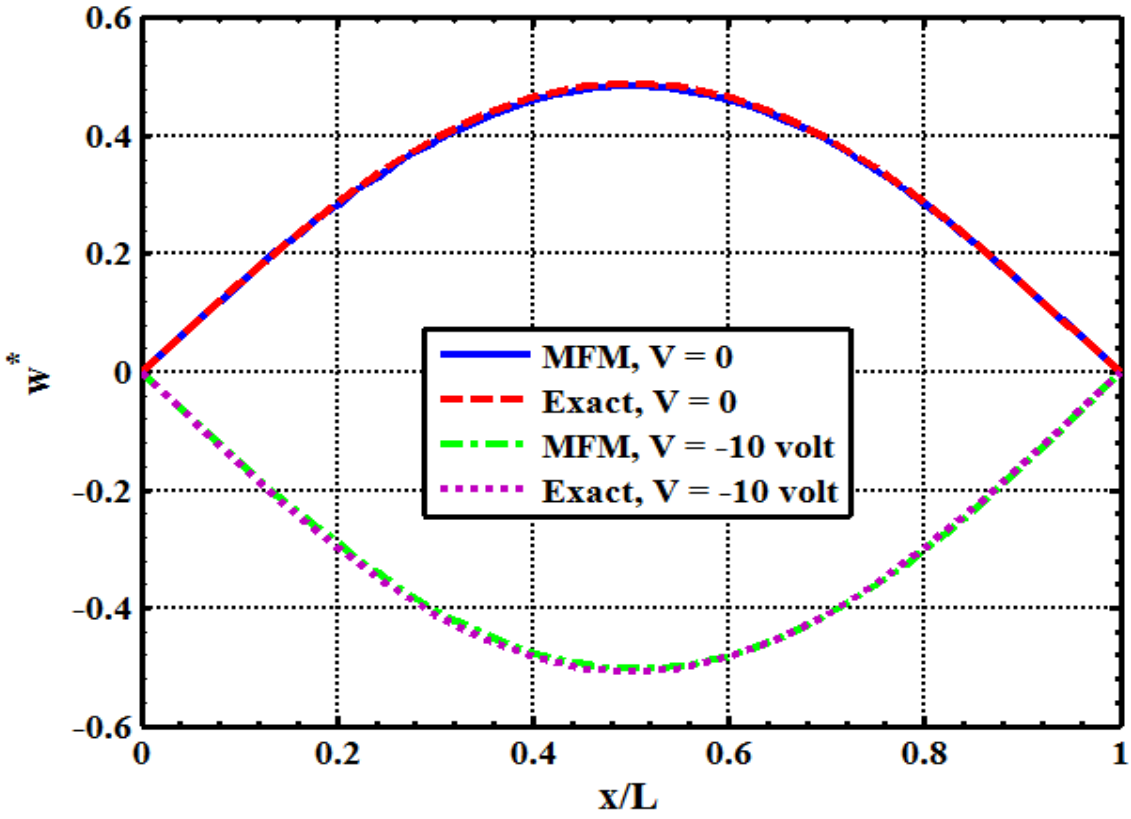

Fig. (5.1) Active static control of shape of a three layered ($0^0/90^0/0^0$) composite beam (s=50, h_p=250 μ m, h=0.005m, $w^* = \frac{100E_T h^3}{q_0 a^4} w(x,0)$, q_0=50N/m^2)

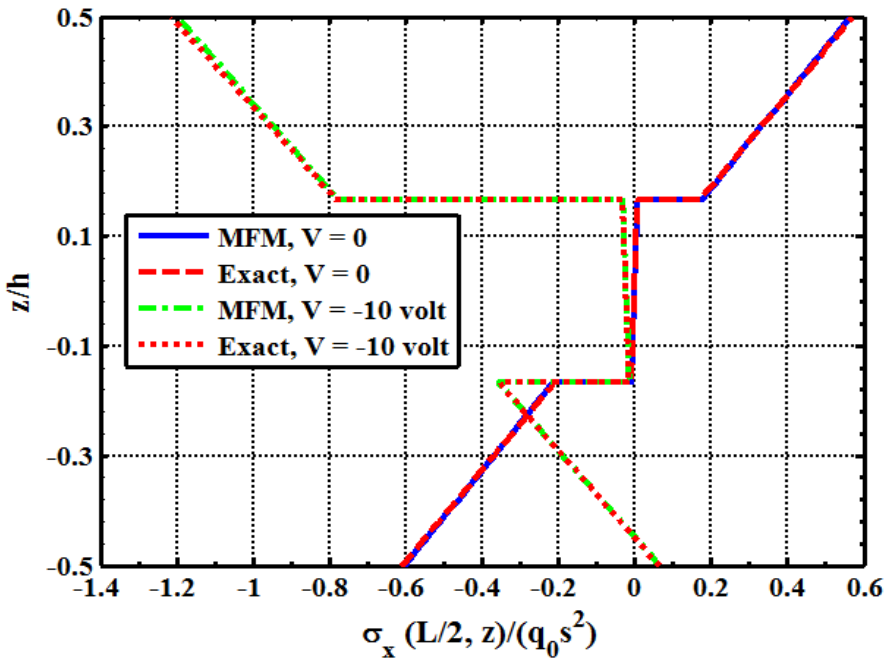

Fig.(5.2) Distribution of the axial stress across the thickness of the three layered ($0^0/90^0/0^0$) composite beam with and without actuated by a piezoelectric layer

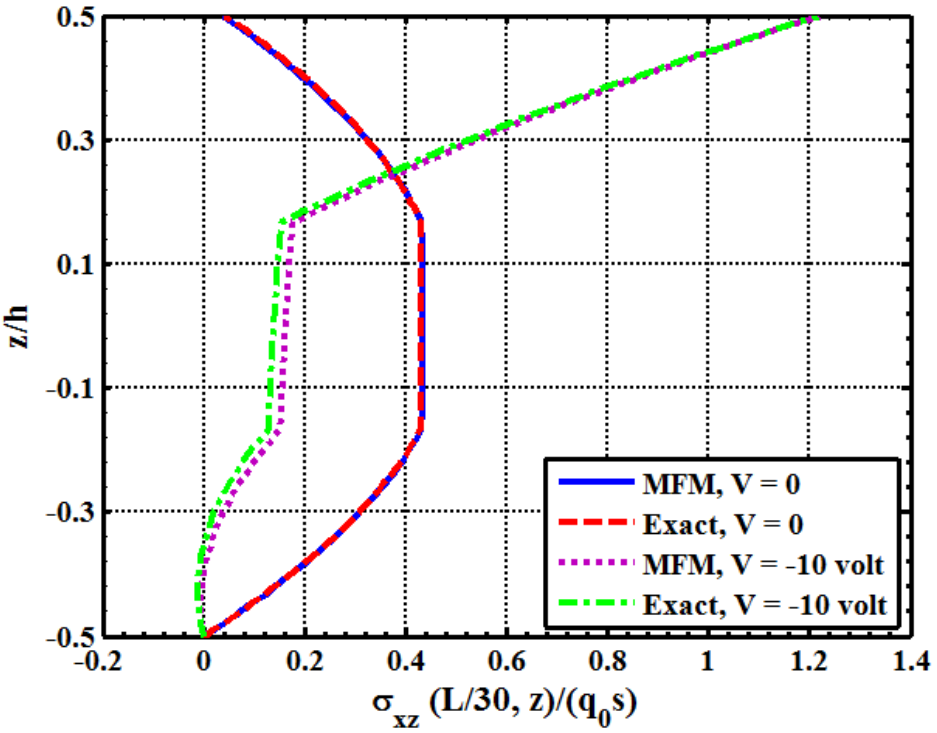

Fig.(5.3) Distribution of the transverse shear stress across the thickness of the three layered ($0^0/90^0/0^0$) composite beam (s=50, h_p =250μ m, h=0.005m, q_0 =50N/m^2)

Comparison of Responses of Mfree Method for Four Layered (0/90/0/90) composite Beam with Exact Solution Method.

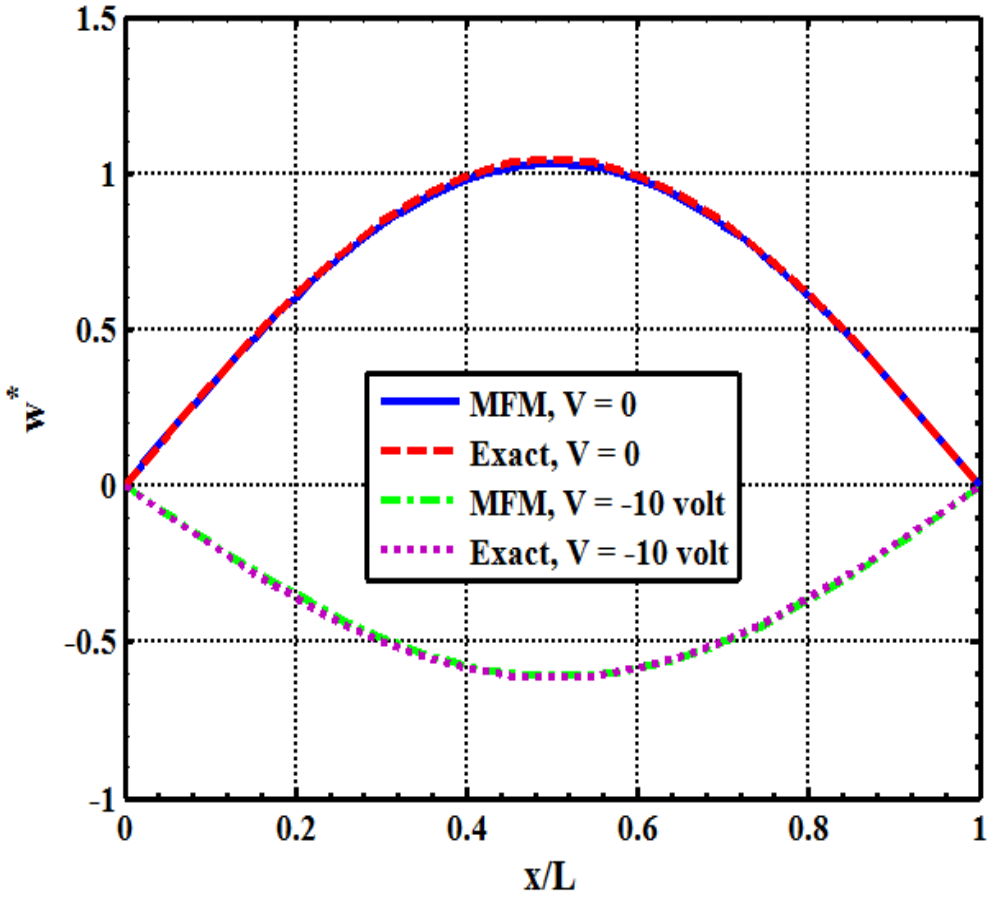

Fig. (5.4) Active static control of shape of a four layered $(90^0/0^0/90^0/0^0)$ composite beam (s=50, h_p=250 μm, h=0.005m, $w^* = \frac{100E_T h^3}{q_0 a^4} w(x,0)$, q_0=50N/m^2)

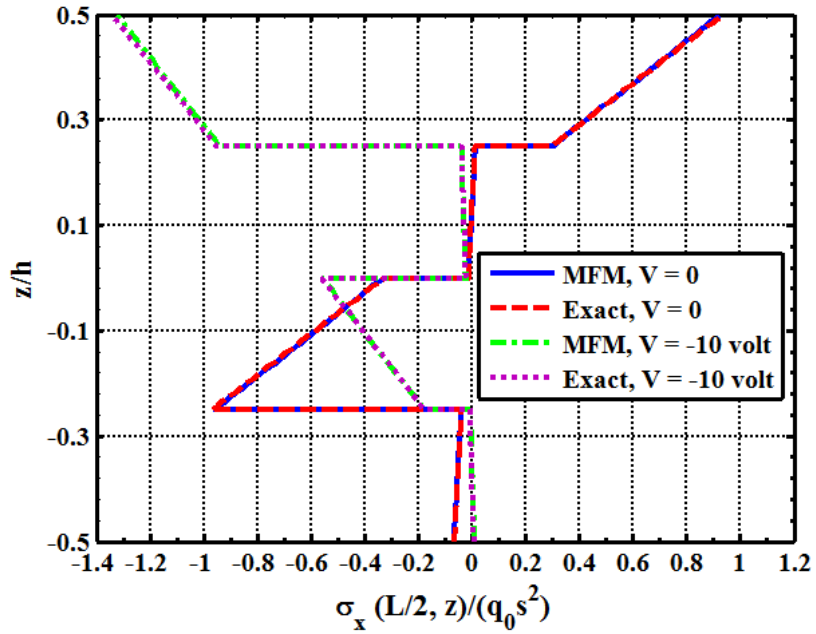

Fig. (5.5) Distribution of the axial stress across the thickness of the four layered ($90^0/0^0/90^0/0^0$) composite beam with and without actuated by a piezoelectric layer (L/h=50, h_p =250 μ m, h=0.005m, q_0 =50N/m ^{2})

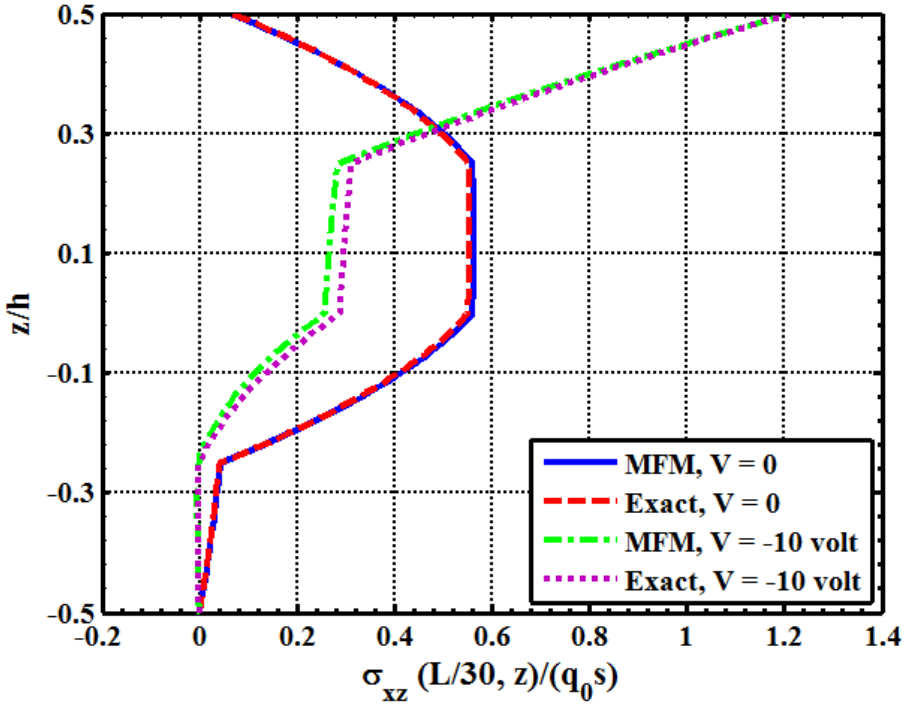

Fig. (5.6) Distribution of the transverse shear stress across the thickness of the four layered ($90^0/0^0/90^0/0^0$) composite beam (s =50, h_p =250 μ m, h=0.005m, q_0 =50N/m ^{2}

6. CONCLUSION AND SCOPE OF FUTURE WORK

In the present work, a new layerwise laminated beam theory based on element free Galerkin (EFG) is proposed to analyze the numerical simulation of piezoelectric laminated beam have been used to verify the validity and precision of the proposed method. The details of the element free Galerkin (EFG) method and its numerical implementation have been presented. It only needs nodes distributed on the upper and lower surfaces of each layer, which avoids the troublesome in generating mesh and saves much preprocess time MLS approximants, which constitute the back bone of the method were described, including several examples. The new approach reduces the dimension of approximation of MLS, which also greatly save the computational cost. The convergence characteristic and accuracy of the method are validated with exact solution. In all the simulations, numeric solutions are insensitive to the EFG-related parameters, which demonstrate the stability of the proposed method.

Meshfree methods are viewed as next generation computational techniques. With evident limitations of conventional grid based methods, like FEM, in dealing with problems of fracture mechanics, large deformation, and simulation of manufacturing processes, meshfree methods have gained much attention by researchers. A number of meshfree methods have been proposed for analyzing complex problems in various fields of engineering. With Mfree methods like EFG it is possible to review developments and applications for various types of structure mechanics and fracture mechanics applications like bending, buckling, free vibration analysis, sensitivity analysis and topology optimization, single and mixed mode crack problems, fatigue crack growth, and dynamic crack analysis and some typical applications like vibration of cracked structures, thermoselastic crack problems, and failure transition in impact problems. Meshfree methods is the possibility of simplifying adaptively and problems with moving boundaries and discontinuities, such as phase changes or cracks.

REFERENCES

[1] Belytschko, T., Y.Y. Lu, and L.Gu (1994), Element Free Galerkin Methods", International Journal for Numeric al Methods in Engineering, 37, 229-256.

[2] Belytschko, T., D. Organ, and Y. Krongauz (1995), A Coupled Finite Element- Element free Galerkin Method", Computational Mechanics, 17, 186-195.

[3] Belytschko, T., Y. Krongauz, M. Fleming, D. Organ and W.K. Liu (1996), Smoothing and Accelerated Computations in the Element-free Galerkin Method", Journal of Computational and Applied Mechanics, 74, 111-126.

[4] Belytschko, T., Y. Krongauz, D. Organ, M. Fleming and P. Krysl (1996), Meshless Methods: An Overview and Recent Developments", Computer Methods in Applied Mechanics and Engineering, 139, 3-47.

[5] Beissel, S. and Belytschko, T. (1996) "Nodal integration of the element-free Galerkin method," Computational Methods Appl. Mech. Eng. 139, 49–74.

[6] Duarte, C.A.M. and Oden, J.T. (1995) "Hp clouds-A meshless method to solve boundary value problems," TICAM Report, 95-05.3

[7] J. Dolbow and T. Belytschko, (1998) "An Introduction to Programming the Meshless Element Free Galerkin Method", Vol. 5, 3, 207-241

[8] Duarte, C.A. and J.T. Oden (1996), H-p Clouds - an h-p Meshless Method, Numeric al Methods for Partial Differential Equations, 1-34.

[9] Lancaster, P. and K. Salkauskas (1981), Surfaces Generated by Moving Least Squares Methods", Mathematics of Computation, 37, 141-158.

[10] Liu,W.K., S. Jun, and Y.F. Zhang (1995), Reproducing Kernel P article Methods", International Journal for Numerical Methods in Engineering, 20 , 1081-1106.

[11] Lu,Y.Y., T. Belytschko and L. Gu (1994), A New Implementation of the Element Free Galerkin Method", Computer Methods in Applied Mechanics and Engineering, 113, 397-414.

[12] Timoshenko, S.P .and J.N. Goodier (1970),Theory of Elasticity (Third ed.). New York, McGraw Hill.

[13] Ray M. C., Mallik N., "Finite Element Solutions for Static Analysis of Smart Structures With a Layer of Piezoelectric Fiber Reinforced Composites", AIAA Journal, vol. 42, no. 7, 2004, pp. 1398-1405, (2004).

[14] Anderson EH, Hagood NW. Simultaneous piezoelectric sensingactuation: analysis and application to controlled structures. Sound Vib (1994).

[15] Donthireddy P, Chandrashekhara K. Modeling and shape control of composite beams with embedded piezoelectric actuators. Compos Struct (1996).

[16] Kapuria S, Sengupta S, Dumir PC. Three-dimensional piezothermoelastic solution for shape control of cylindrical panel. J Thermal Stresses (1997).

[17] Crawley, E.F. and Luis, J.D., Use of piezoelectric actuators as elements of intelligent structures, American Institute of Aeronautics and Astronautics Journal 25(10), 1373–1385, (1987).

[18] Lee, C.K., Chiang, W.W. and Sulivan, Piezoelectric modal sensor/actuator pairs for critical active damping vibration control, Journal of the Acoustical Society of America 90, 374–384, 1991).

[19] J.N. Reddy, On laminated composite plates with integrated sensors and actuators. Engineer structure. 1999; 21: 568-593.

[20] Uchino K. Recent topics of ceramic actuators: How to develop new ceramic devices. Ferroelectrics. 91: 281-292,1989.

[21] Liu GR, Gu YT. An Introduction to Meshfree Methods and Their Programming, Springer, Nethe[16] Tzou HS, Ye R. Analysis of piezoelectric structures with

[22] Tzou HS, Ye R. Analysis of piezoelectric structures with laminated piezoelectric triangle shell element. AIAA Journal, 34: 110-115, 1996.

[23] Yuan XSH, Chen FJ, Yao LQ. Subdomain collocation method for multilayered piezoelectric material. Proceedings of SPAWDA.441-446, 2010.

[24] Crawley EF, Anderson EH. Detailed Models of Piezoceramic Actuation of Beams. Journal of Intelligent Material Systems and Structures. 1: 4-25, 1990.

[25] Crawley EF, de Luis J. Use of piezoelectric actuators as elements of intelligent structures. AIAA Journal. 25: 1373-1385, 1987.